PONTIFÍCIA UNIVERSIDADE CATÓLICA
DO RIO DE JANEIRO

Débora Cristina Ferreira da Silva

Non-Newtonian flow displacement in well operations

Dissertação de Mestrado

Dissertation presented to the Programa de Pós-Graduação em Engenharia Mecânica of PUC-Rio in partial fulfillment of the requirements for the degree of Mestre em Engenharia.

Advisor: Profª. Mônica Feijó Naccache
Co-advisor: Prof. Hans Joakim Skadsem

Rio de Janeiro
September 2024.

Débora Cristina Ferreira da Silva

Non-Newtonian flow displacement in well operations

Dissertation presented to the Programa de Pós–graduação em Engenharia Mecânica of PUC-Rio in partial fulfillment of the requirements for the degree of Mestre em Engenharia Mecânica. Approved by Examination Commitee.

Profª. Mônica Feijó Naccache
Advisor
Pontifícia Universidade Católica do Rio de Janeiro - PUC-Rio

Prof. Hans Joakim Skadsem
Co-advisor
Universidade de Stavanger - UiS

Dra. Priscilla Ribeiro Varges
Pontifícia Universidade Católica do Rio de Janeiro - PUC-Rio

Prof. Diogo E. V. Andrade
Universidade Federal do Rio Grande do Sul - UFRGS

Prof. Knut Erik T. Giljarhus
Universidade de Stavanger - UiS

Rio de Janeiro, September 23rd, 2024

Débora Cristina Ferreira da Silva

MBE in Energy from Department of Mechanical Engineering - PUC-Rio - in 2020; Graduated in Petroleum Engineering from Estacio de Sá University - UNESA - in 2016. Main areas of interest: Fluid Mechanics; Flow displacement; Through-Tubing Abandonment (TTA).

A Deus pela minha vida e saúde. A minha
família pelo amor incondicional.

Acknowledgement

I would like to extend my heartfelt gratitude to my family, my mother Márcia my father Eduardo, my brother Eduardo Jr, my nephews Eduardo Alves and Bernardo and my wife Lígia for always giving support, encouragement and love throughout my journey.

To my advisor, Professor Mônica Naccache, and my co-advisor, Professor Hans Joakim, I would also like to express my deep gratitude. Your invaluable guidance, support, and insightful suggestions have been essential throughout this process. I am truly grateful for your kindness and support during this time, and I feel extremely fortunate to have had such brilliant professors leading me through this master's dissertation.

All my gratitude to all my colleagues at the Norwegian Research Centre (NORCE), including Samuel, Daniel, Gunnar, Katherine, Erlend, and Camila. Their support was undoubtedly crucial in helping me complete my master's program.

A special thanks to Victor Nogueira, that is more than a friend, he became a brother that I have in Norway. Thanks for our funny moments and laughs.

A big thanks to my wonderful friends at PUC-Rio, Elisa, Bruno Jorge and Leonardo for the countless hours we spent studying together.

A special thanks to my great friend Elaine Marcela, for your friendship throughout all these years.

I also want to thank NORCE and BRANOR for providing all the infrastructure to conclude this master's thesis.

To the professors who participated in the Examining Committee.

To all the professors and staff of the Mechanical Department for their teaching and help.

Abstract

Silva, Débora Cristina Ferreira da; Naccache, Mônica Feijó (Advisor); Skadsem, Hans Joaquim (Co-advisor). **Non-Newtonian flow displacement in well operations**. Rio de Janeiro, 2024. 76p. – Department of Mechanical Engineering, Pontifical Catholic University of Rio de Janeiro.

Several oil industry operations, such as plugging and abandonment wells, cementing operations, and restarting flows of gelled pipes, use the displacement of one fluid by another in annular tubes. There are many variables that can affect the displacement efficiency, namely the rheological behavior of the fluids, the density ratios, and the well geometry. The interaction of these parameters can lead to instabilities at the interface between fluids that will result in inefficient flow displacement processes. In these circumstances, an effective procedure is required to prevent issues that could result in dangers and significant financial losses. In this work we present experimental results of displacement efficiency through an annular tube. The analysis is done for low Reynolds numbers, with a Newtonian (water) fluid being displaced by a non-Newtonian (xanthan gum solution) one, to simulate a plug & abandonment operation. The experimental study is done using a test rig that consists of a steel tubing and a transparent casing with diameters that reflect a real-case scenario. We study the displacement process using two different inclinations, concentric and eccentric geometries, and tubing vibration. To assess the impact of these parameters on displacement efficiency, we perform flow visualization at the experimental rig and evaluate interface instability.

Keywords

Resumo

Silva, Débora Cristina Ferreira da; Naccache, Mônica Feijó (Orientadora); Skadsem, Hans Joaquim (Coorientador). **Deslocamento de fluxo não-newtoniano em operações de poço**. Rio de Janeiro, 2024. 76p. Dissertação de Mestrado – Departamento de Engenharia Mecânica, Pontifícia Universidade Católica do Rio de Janeiro.

Diversas operações da indústria petrolífera, como o fechamento e abandono de poços, operações de cimentação e reinício de escoamento em tubos gelificados, utilizam deslocamento de um fluido por outro em tubos anulares. Existem muitas variáveis que podem afetar a eficiência do deslocamento, nomeadamente o comportamento reológico dos fluidos, as relações de viscosidade e densidade e a geometria do poço. A interação desses parâmetros pode levar a instabilidades na interface entre os fluidos, resultando em processos de deslocamento de fluxo ineficientes. Nessas circunstâncias, é necessário um procedimento eficaz para prevenir problemas que possam resultar em perigos e perdas financeiras significativas. Neste trabalho, apresentamos resultados experimentais da eficiência de deslocamento por um tubo anular. A análise é realizada para números de Reynolds baixos, com um fluido newtoniano (água) sendo deslocado por um fluido não newtoniano (solução de goma de xantana), simulando uma operação de fechamento e abandono de poço. O estudo experimental é realizado usando um dispositivo de teste que consiste em um tubo de aço e uma carcaça transparente com diâmetros que refletem um cenário real. Estudamos o processo de deslocamento usando duas inclinações diferentes, geometrias concêntricas e excêntricas, e vibração de tubulação. Para avaliar o impacto desses parâmetros na eficiência de deslocamento, realizamos visualização de fluxo no equipamento experimental e avaliamos a instabilidade da interface.

Palavras-chave

Deslocamento de fluido não newtoniano; Operações de Cimentação; Abandono através do tubo

Table of Contents

List of Figures

List of Tables

List of Symbols

Aa = Annulus cross-sectional area, m

At = $\frac{\rho_1 - \rho_2}{\rho_1 + \rho_2}$; Atwood number

$\forall_a$ = Annular volume, m^3

η^* = Characteristic viscosity, N*s/m^2

$\bar{V}$ = Characteristic velocity, m/s

t_c = Characteristic time, s

p* = Dimensionless pressure

r^* = Dimensionless radio, m

x^* = Dimensionless Longitudinal direction

u^* = Dimensionaless velocity in x direction

t^* = Dimensionless Time

D_h = Hydraulic Diameter, m

Do = Outer diameter, m

Di = Inner diameter, m

x = Longitudinal direction, m

p = Pressure, Pa

ρ_1 = Density (Water), kg/m^3

ρ_2 = Density (Xantham Gum), kg/m^3

q_1 = Flow rate (1)

q_2 = Flow rate (2)

Re = Reynolds number

r = Ratio, m

μ = Shear viscosity, Pa. s

τ = Shear stress, Pa

$\dot{\gamma}$ = Shear rate, s^{-1}

t = Time, s

u = Velocity in x direction, m/s

v_1 = Velocity (1) in r axis, m/s

v_2 = Velocity (2) in r axis, m/s

η$_2$ = Viscosity, N*s/m^2

η$_c$ = Viscosity of Xanthan Gum, N*s/m^2

η$_1$ = Viscosity of Water, N*s/m^2

$\dot{\gamma}_1 = v_1/D_h$; Shear rate for v_1

$\dot{\gamma}_2 = v_2/D_h$; Shear rate for v_2

*One day, when you look back, you will see that the most beautiful days were
the ones when you fought.*

Sigmund Freud

1. Introduction

The displacement of complex fluids is critical in various industrial processes, particularly in oil well plugging, abandonment, and cementing operations. When the wells achieve the end of their production lives, they must be plugged and abandoned. Cementing operations aim to establish permanent zonal isolation and a hydraulically sealed well. The desired outcome is achieved by displacing or removing the in-situ drilling fluids using a series of displacing fluids, such as spacers and cement slurries, within a narrow, elongated confined annulus geometry (Eslami et al. [1]).

However, this is not an easy task to accomplish, as many variables can affect displacement efficiency. Geometry, flow parameters, and fluid rheology are critical factors in fluid displacement. Eccentric annular spaces can lead to uneven flow, resulting in bypassed zones and trapped fluids. Flow parameters, such as injection rate and pressure, impact the speed and force of displacement, with high rates potentially causing turbulence and low rates leading to inefficiency. Fluid rheology, particularly viscosity, plays a key role, as high-viscosity fluids may resist flow, while low-viscosity fluids can cause channeling. The hierarchy refers to the relative dominance or influence of these factors - such as viscosity, density, and rheology - and how these differences shape the interaction between fluids during displacement. Understanding these interactions is essential for optimizing the process (Skadsem et al. [2]).

The main geometric challenges in well construction include eccentricity, which leads to uneven fluid distribution and affects cement placement, and well inclination, which impacts fluid dynamics and zonal isolation (Figure 1). Flow parameters, particularly inertia and buoyancy forces, play crucial roles in fluid movement, influencing how quickly fluids respond to flow changes and how well lighter fluids can rise against heavier ones. Additionally, the non-Newtonian behavior of fluids, characterized by shear thinning and yield stress, complicates flow and mixing, making it essential to consider these factors during cementing operations to ensure effective displacement and bonding (Moroni et al. [3]).
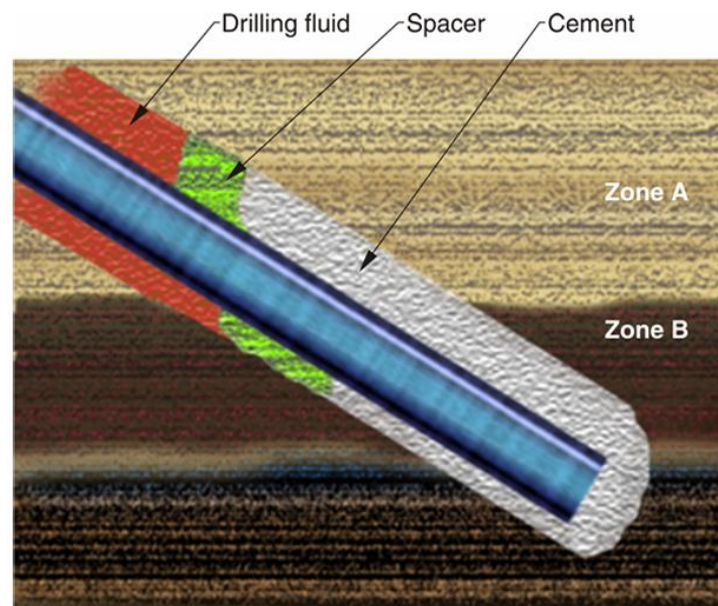
Figure 1 - Drilling fluid and spacer fluid being displaced by cement slurry (Moroni et al.[3]).

In these cases, fluids such as brine or drilling mud must be efficiently displaced by a cement slurry through the annular space of the wellbore. If the drilling fluid and spacer are not completely removed, it can compromise zonal isolation, which is essential for preventing fluid migration between subsurface zones. Inadequate displacement may result in incomplete sealing, creating channels or voids where fluids can migrate, increasing the risks of blowouts, environmental damage, and long-term well-being integrity issues. Achieving perfect displacement is not just a procedural goal but a critical factor for operational success. Proper fluid displacement ensures uniform cement bonding, providing a reliable barrier throughout the well's life. Failure to achieve this compromises safety, environmental sustainability, and the overall viability of the operation, highlighting the importance of precise control over displacement parameters (Moroni et al. [3]).

To address the challenge of displacing fluid on the narrow side of the annulus, the industry has recently introduced devices that generate both lateral and axial vibrations within the tubing, reducing the risk of poor displacement (Figure 2). Additionally, rotating the casing during cementing significantly improves displacement efficiency along the narrow side of the annulus. This rotation (Figure xx) helps evenly distribute the cement slurry around the wellbore, reducing the chances of channeling or voids that could compromise zonal isolation.

As a result, casing rotation ensures a more uniform cement job, enhancing the long-term integrity and reliability of the well (Bu et al. [4]).
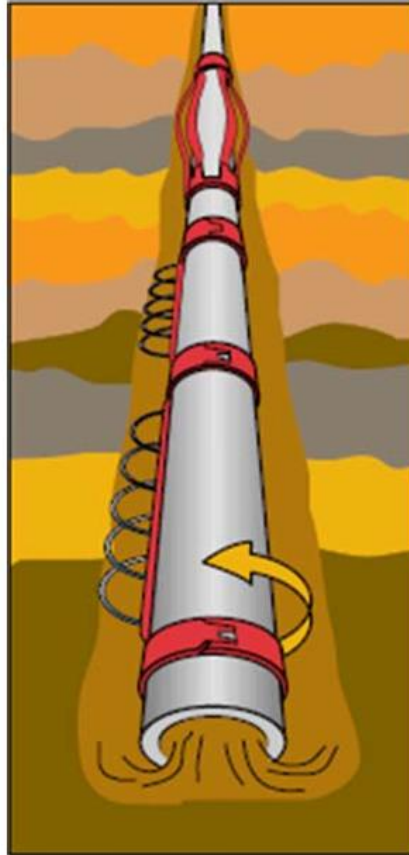
Figure 2 - Tubing vibration during displacement (Moroni et al.[3])

This experimental study examines the fluid displacement process, simulating scenarios typical of Plug & Abandonment (P&A) operations. The experimental tests are conducted using one concentric (0%) and two eccentric geometries (62% and 75%), two different inclinations (0º and 60º) and the introduction of tubing vibration at frequency 5 Hz to analyze their effects on displacement efficiency.

Two fluids were utilized in this study: a yield stress fluid (Xanthan Gum dyed blue) to represent a cement slurry and tap water as a Newtonian fluid to simulate brine, both of which are common in Plug and Abandonment (P&A) processes. This research investigates how factors such as geometry, inclination, and vibration affect the flow behavior and interaction between these fluids. The findings aim to optimize displacement operations, ensuring the complete removal of the displaced fluid and facilitating effective zonal isolation.

1.1. Motivation

This research is motivated by the deeper exploration and comprehension of the Plug and Abandonment operations.

According to Ytrehus et al. [5], improper annular cementing can lead to severe consequences, such as leakage during the production phase and significant costs during well abandonment. Such leakage compromises well integrity and poses environmental risks, including groundwater contamination. Additionally, inadequate cement placement can result in costly remediation efforts and regulatory fines. To minimize these risks, it is crucial to employ optimal cement placement procedures, which require a deeper understanding of fluid displacement dynamics within the wellbore annulus. Factors such as fluid properties and annular geometry significantly influence cement effectiveness. Since all wells are typically cemented in multiple sections, improving cementing practices is particularly relevant for numerous operations conducted annually.

By addressing these complexities, this experimental study aims to contribute valuable insights that will help safety, cost-effective and reliability of P&A well operations, ultimately leading to improved environmental stewardship and sustainability in the oil and gas sector.

1.2. Objective

In the Oil and Gas industry, pipe mechanical vibration is employed during cementing operations to enhance fluid displacement in Through-Tubing Abandonment (TTA) process. However, this research seeks to evaluate the effectiveness of this method in diverse conditions. Specifically, it examines whether the vibration technique benefits scenarios characterized by low Reynolds numbers.

To thoroughly investigate displacement efficiency, we conducted downscaled experimental tests in a laboratory setting. These tests involved displacing Newtonian fluid with a non-Newtonian fluid while varying parameters such as inclination, eccentricity, Reynolds numbers and tubing vibration to study fluid displacement efficiency.

1.3. Structure of the thesis

The structure of the document begins with Chapter 1, introduces the research topic which includes the introduction, motivation, objectives, and limitations. Chapter 2 follows with a bibliographical review which offers a comprehensive literature review, summarizing previous research on fluid displacement, cementing techniques, and factors affecting cement placement. Chapter 3 details the research methodology, including the experimental setup, materials, and techniques for data collection. Chapter 4 describes the experimental plan, detailing the specific experiments conducted, the variables tested, and how they simulate real-world cementing conditions. The results and discussions are presented in Chapter 5. Chapter 6 concludes the document, and Chapter 7 brings suggestions for future work. Finally, Chapter 8 provides the bibliographic references. This document also brings Appendix A and B.

1.4. Limitation

The experimental conditions examined within this research have the viscosity and density fluids, pump workflow and rig length as a boundary.

The tests were conducted with low density and low viscosity fluid being displaced in a downscaled experimental test rig. Additionally, a low-velocity pump supply was employed, resulting in a low workflow rate. This research was limited to analyzing laminar flow patterns and did not extend its scope to include situations characterized by high flow velocities and viscosity, turbulent flow regimes, immiscible fluids, or fluids prone to hardening.

The experiments aimed to replicate the pipe diameter ratio and considered similarity through dimensionless numbers. However, a significant limitation is the lack of dynamic equivalence to field conditions. Despite using lower velocities and flow rates, the primary issue is the absence of full-scale similarity when compared to real case scenario (Appendix B).

2. Bibliographical Review

Cementing operations for plug and abandonment (P&A) in the oil and gas industry involve a series of steps to safely and permanently seal wells that are no longer in use. The primary objective is to isolate the wellbore from surrounding formations to prevent fluid migration and environmental contamination. This process includes planning, regulatory compliance, setting cement plugs at various depths, preparing and pumping cement slurries, verifying cement quality, and removing wellhead and surface equipment (Vrålstad et al. [6]).

The main goal is to restore the natural barriers that were disrupted during the well drilling process, particularly the caprock and low permeability overlying formations. Therefore, when abandoning the well, these barriers must be restored by placing cross-sectional cement plugs within the wellbore (Tao et al. [7]).

Several works have been analyzing the problem throughout the years, both numerically and experimentally (e.g., Lockyear et al. [8]; Jacobsen et al. [9]; Tehrani et al. [10]; Pelipenko and Frigaard [11], Malek Mohammadi et al. [12]; Ytrehus et al. [5]), but there are still several lacks in the literature, mostly due to the large number of important parameters influencing the flow displacement.

Regarding fluids rheology, it was observed that flow displacement of yield stress fluids can lead to unyielded regions, static fluid layers close to the walls and viscous fingering instabilities Moyers-Gonzalez and Frigaard [13]; Denn and Bonn [14]; Lindner et al. [15]. Aranha et al. [16] numerically investigated how to optimize density and viscosity hierarchy to avoid fluids contamination during displacement and analyzed the effect to string rotation on the displacement efficiency.

The effect of eccentricity and density difference was studied in Teharani et al. [17]. The interface between the fluids were investigated in Ytrehus et al. [18] and Lund et al. [19] for inclined and irregular geometries. Skadsem et al. [20] analyzed experimentally the cementing displacement in critic conditions of irregular wells with highly inclined geometries and large eccentricity. The displacement through irregular geometries was also analyzed in Roustaei and Frigaard [21], Roustaei et al. [21], Skadsem et al. [22], Varges et al. [23] and Varges

et al. [24]. The presence of a washout zone generates unyielded zones that compromise the displacement efficiency.

The main issues regarding geometry include eccentricity and well inclination. In respect of flow parameters, inertia, and buoyancy forces play an important role, while fluids rheology is also a challenge due to the non-Newtonian fluid behavior, including shear thinning and yield stress of one or both fluids (Moroni et al. [3]).

2.1. Well Cementing Operations for permanent Abandonment

The process of well abandonment is labor-intensive and expensive procedure, and there is a substantial global demand to securely plug and decommission numerous offshore wells in the coming years (Vrålstad et al. [6]).

The well cementing process involves two main operations: primary cementing and remedial cementing. Primary cementing is the initial and crucial step in the cementing process. During this stage, a cement sheath is placed in the annulus between the casing and the formation. This step is performed during the construction of the well and focuses on isolating the annulus outside the casing string with the purpose of ensuring zonal isolation to prevent fluid migration, provide structural support for the well, protect the casing from corrosion, and enhance safety by creating a secure barrier. Following primary cementing, remedial cementing takes place, during which engineers inject cements into specific well locations for purposes like well repair and abandonment (Kamali et al. [25]).

Moreover, oil and gas wells inevitably require eventual plugging and abandonment. Improperly sealed wells can imply environmental risks if not handled correctly. Plugging materials (barriers) may fail due to natural fractures, faults, tectonic stress, or incorrect placement or choice of materials. The success of a P&A operation depends on the choice of plugging material and the precision of the placement technique employed. Techniques for placing cement plugs vary and include the balanced method, dump-bailer method, two-plug method, and jet grouting (Khalifeh [26]).

2.1.1. Throught Tubing Abandonment (TTA)

A cost-effective and time saving alternative for P&A (Plug and Abandonment) operations is to achieve isolation by installing a cement plug through the tubing. This procedure is known as through-tubing abandonment (TTA), where the tubing remains in the well and consists in cutting the production tubing and cementing it within the production casing, establishing a thorough cross-sectional barrier in the wells (Figure 3). A concern associated with this method is whether the cement will effectively displace the initial fluid, given potential issues related to tubing centralization and unfavorable flow dynamics within the annulus (Skadsem et al. [2]).
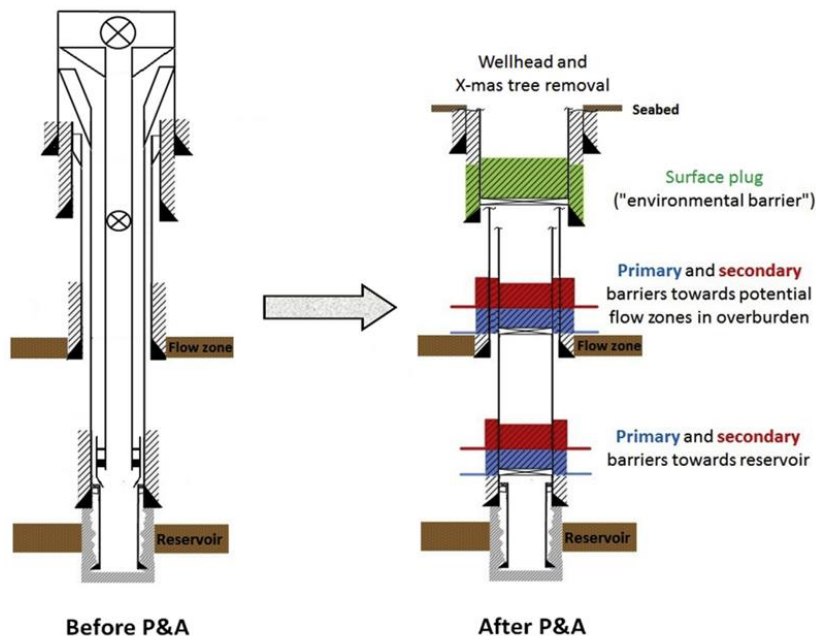
Figure 3 - Simplified illustration of a typical offshore production before and after P&A. The color coding for primary barriers (blue), secondary barriers (red), and surface plug (green) is based on current Norwegian well barrier definitions (Vrålstad et al. [9])

The plugging and abandonment (P&A) process involves circulating high-density drilling fluid and installing a deep-set mechanical plug initially. Barriers are established to isolate fluid-bearing formations, including high-pressure zones and hydrocarbon-containing formations. An environmental barrier, known as an open hole-to-surface plug, is placed below the seabed to prevent residual fluid contamination. Subsequently, the conductor and wellhead are removed. Oil & Gas

UK (2015a) outlines three phases of P&A operations: Reservoir abandonment (Phase 1), Intermediate abandonment (Phase 2), and Wellhead and conductor removal (Phase 3). An additional phase, "Preparatory work" (Phase 0), is proposed to cover pre-P&A activities (Vrålstad et al. [6]).

Egbert Van Riet et al. [27] highlight several challenges inherent to through-tubing abandonment (TTA). Firstly, production tubing often lacks centering within the casing, resulting in significant eccentricity. Secondly, the presence of measurement cables or control lines attached externally to the production tubing adds complexity, as regulatory requirements may demand their removal before cementing. Ensuring the cement outside the casing forms a reliable barrier is crucial for effective TTA; uncertainties regarding the quality of this external cement can complicate operations significantly. Therefore, meticulous selection of well candidates, thorough planning, and sometimes specialized methodologies or technologies are essential to mitigate the risks associated with improper cement placement in TTA operations.

According to Thom et al. [28], the initial plan for abandoning a subsea field involves a pre-abandonment work using a Light Well Intervention Vessel (LWIV), followed by the complete Plug and Abandon (P&A) operation with a Mobile Offshore Drilling Unit (MODU). They worked in a case of study in the Central North Sea, UK. This field included four subsea wells drilled between 1997 and 2007. All four wells produced naturally without artificial lift, resulting in a liquid-filled A-annulus three wells with inhibited seawater and the fourth with base oil. Each of these wells was chosen as a candidate for Through-Tubing Abandonment (TTA), allowing consistent operational techniques to be applied across the entire field.

The process of installing the TTA cement plug begins by circulating cement down through production tubing. This ensures that the cement moves efficiently through the tubing, into the wellbore, and toward the desired placement location. Returns are taken from the annulus, the space between production tubing and casing, which allows for the controlled flow of displaced fluids as the cement is introduced. The cement plug is strategically placed above both the production packer and the deep-set plug, which are already positioned in the well to provide isolation and support. To enhance cement distribution in the annulus, an agitator tool is used within the tubing, promoting even coverage and adhesion. This process

helps ensure a more reliable seal, reducing the chances of gaps or fluid migration, thereby improving well integrity and zonal isolation during abandonment operations (Thom et al. [28]).

Overall, these steps not only ensure the integrity of the well but also contribute to efficient and effective abandonment operations, minimizing the potential for future fluid migration or integrity issues in the wellbore.

Figure 4 shows a schematic of Through Tubing Abandonment.
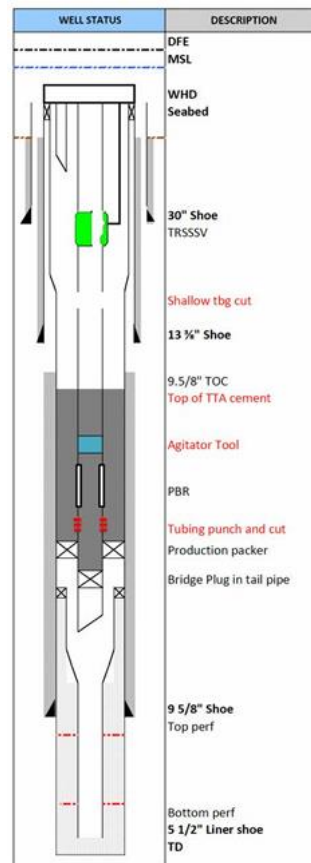
Figure 4 - TTA schematic example (Thom et al. [31])

The case of study from Thom et al. [29] with through-tubing abandonment (TTA) operations from a Light Well Intervention Vessel (LWIV), has demonstrated be more efficient than traditional methods involving LWIVs and Mobile Offshore Drilling Units (MODUs). Despite requiring MODU for installing a shallow environmental cement plug, future advancements aim to enable complete well abandonment from LWIVs by adapting techniques like laying tubing sections on

the seabed. Ongoing improvements focus on optimizing cement design and compatibility with wells equipped with PDHG cables.

Aas et al. [19] has demonstrated through full-scale experimental tests that good cement placement can be achieved when the tubing is left in the hole. The work showed this is true both with and without control lines attached to the tubing. Full-scale tests were conducted with several assemblies of 7" tubing cemented in 9 5/8" casings to determine the sealing ability of annulus cement when the tubing is left in the hole. These tests used both conventional and expandable cement and were performed with and without control lines present (Figure 5). One test series used conventional cement, while another used expandable cement

Figure 5 - Cut test assemblies with conventional cement. On the left, with control lines; on the right, without control lines (Aas et al. [21]).

The experiments conducted by Aas et al. [19] demonstrate that cement can be effectively placed in the annulus even when the tubing remains in the hole (Figure 6). During the two series of full-scale cement placement experiments, researchers detected some micro annuli, which are relatively small and likely non-uniform. This irregularity suggests that these micro annuli would not allow significant leakage rates in practical plug and abandonment (P&A) operations, especially considering the axial length of the cemented annulus, which provides ample coverage and support.

Moreover, the tests indicate that the presence of control lines did not introduce any additional leakage paths, further reinforcing the reliability of cement placement in these scenarios. Overall, these findings underscore the effectiveness of leaving the tubing in place during cementing operations while minimizing

potential leakage, thus contributing to enhancement integrity of the well during abandonment processes.

Figure 6 - Cut test assemblies with expandable cement without control lines (left) and with control lines (right) (Aas et al. [21]).

This technique aims to enhance HSSE (Health, Safety, Security, and Environmental) outcomes by leaving tubing in the well during decommissioning. This eliminates the necessity to suspend the well or utilize a drilling Blowout Preventer (BOP) for recovery operations (Aas et al. [19]).

By avoiding these activities, the approach aims to reduce the risk of incidents associated with tubing retrieval and handling.

2.1.1.1. Tubing vibration

The industry has recently introduced agitator tools to generate lateral and axial vibrations within tubing. These tools are employed to effectively mitigate adverse displacement conditions encountered during operations. Some commercial tools generate both axial and lateral agitation due to the moving masses and pistons inside the tool, which are driven by fluid flow. This hydraulic action increases the amplitude and frequency of the agitation as pumping speed increases. Therefore, to achieve high amplitude and frequency, a faster pumping rate is required. Axial vibration resembles the reciprocation of the casing, but with a much higher frequency. The lateral movement, similar to that created by downhole equipment, can aid in fluid displacement, especially if rotational movement of the pipe along

the inner casing wall is possible. This can help circulate fluids around the entire annulus and potentially reduce the risk of channeling on one side (Skadsem [2]).

Comprehensive experimental tests on deviated wellbores was studied by S.R.Keller et al. [30] , with angles of 80 degrees from the vertical. The primary goal was to explore the potential enhancements in displacement efficiency applying tubing rotation and reciprocation. Various test scenarios were executed, leading to the conclusion that both pipe rotation and reciprocation could indeed substantially improve the efficiency of displacing settling drilling fluid in inclined wells (Fredheim [31]).

In a notable publication on vibration, Thom et al. [29] conducted a comprehensive field study on rig-less subsea well abandonment in the North Sea, focusing on the application of vibration technology. Their study involved the deployment of a specialized vibration tool installed within the production tubing. This tool was designed to generate oscillation waves in the flow, specifically aimed at enhancing cement coverage and improving displacement efficiency in the annulus. The research findings underscored several key benefits of employing vibration tools in well abandoned operations. Firstly, the oscillation waves facilitated better fluid displacement, ensuring more thorough cement placement and improved zonal isolation. Secondly, by enhancing cement coverage in the annulus, the tools contributed to mitigating risks associated with incomplete displacement and potential fluid channeling.

Moreover, Thom et al. [29] demonstrated the practical feasibility and effectiveness of vibration tools in real-world subsea environments, highlighting their potential to reduce operational time and costs while enhancing safety and environmental performance. This study has encouraged further interest and investment in vibration technology as a valuable tool for optimizing abandonment procedures and improving overall well integrity management in offshore operations.

Skadsem et al. [2] conducted experiments on annular fluid displacement using an apparatus that enabled lateral movement of the inner tubing. Their findings showed that vibration effectively enhances displacement at inclinations from vertical to 80 degrees. High-frequency vibrations were more effective than lower-frequency ones at the same amplitude, and their analysis revealed a correlation between higher flow rates and increased vibration amplitudes.

2.2. Fluid Properties and Operational Conditions for Cementing

Studies on displacement mechanics began in the 1940s, with Jones and Berdine [18] identified critical factors influencing the displacement process in vertical wellbores. These factors include drilling fluid condition, pipe movement (such as reciprocation and casing/liner rotation), pipe centralization, flow rate, and density differences between fluids. Factors influencing displacement fall into two main categories: driving factors, such as increased frictional pressure drop, buoyancy force, drag force, and tubing movement, which aid displacement; and resistance factors, such as density and viscosity hierarchies, which hinder displacement. High gel strength and yield stress of the displaced fluid can also impede displacement. Additionally, eccentricity can reduce displacement efficiency by limiting the mobility of displaced fluid in narrow annular sections (Foroushan et al. [18]).

2.2.1. Rheological Properties

Along the years, researchers have investigated the rheological properties of both displacing and displaced fluids, aiming to understand the influence of viscosity on displacement and interface properties. According to Foroushan [18] , efficiency of the displacement process can be enhanced by reducing the viscosity of the displaced fluid.

Cement slurries, preflush fluids and drilling fluids often exhibit non-Newtonian behavior, with cement slurries displaying complex rheological features like yield stress, shear-thinning, and time-dependent properties. Drilling fluids, designed for specific functions, are typically shear-thinning fluids with a yield stress, making them resistant to stress during the displacement process. The yield stress causes the fluid to adhere to the walls, making it challenging to remove. Unlike purely viscous displacement flows, yield stress fluid displacements can result in static residual layers on the walls, reducing the efficiency of fluid displacement and removal, in contrast to the ideal efficiency of 100 % (Guillot and Nelson [32]).

In wellbore operations, the interplay between fluid density and viscosity is crucial for efficient displacement. Research indicates that a high viscosity ratio

(ηdisplacing/ηdisplaced) improves the displacement process by creating a more stable displacement front and enhancing sweep efficiency (Couturler [33]).

One prominent instability is the Saffman–Taylor instability, also known as viscous fingering, which occurs when injecting a less-viscous fluid into narrow confined spaces (e.g., the annulus) to replace a more-viscous in-situ fluid. This process results in the formation of finger-like interfacial patterns, leading to a notable reduction in displacement efficiency during cementing operations (Bugrayev [34]; Aghajannezhad et al. [35]; Eslami et al. [36].

Studies by Flumerfelt [37] , Nguyen et al. [38], Tehrani et al. [17], Miranda et al. [23], Aranha et al. [16] , and Foroushan et al. [18], among others, have provided a deeper understanding of how these rheological properties interact during displacement. The careful balance of fluid properties is crucial for enhancing displacement efficiency and improving overall wellbore stability and integrity. Research by Lockyear et al. [8] emphasizes the importance of comprehensive planning and optimization of these properties to ensure successful outcomes in well abandonment and cementing operations.

2.2.1.1. Viscosity of a non-Newtonian Fluids

Non-Newtonian fluids have a non-linear relationship between shear stress and shear rate, setting them apart from Newtonian fluids. Their viscosity can change with temperature and pressure, exhibiting either shear thinning (decreasing viscosity with increased shear rate) or shear thickening (increasing viscosity). This shear thinning behavior is common in drilling fluids, cement slurries, and heavy oils. In the well cementing industry, non-Newtonian fluid behavior is described using three main mathematical models: the Power-law model, the Bingham model, and the Herschel-Bulkley model. The Herschel-Bulkley model integrates power-law and Bingham plastic behaviors, requiring yield stress to be surpassed for flow to initiate, after which shear rate and shear stress follow a power-law relationship. (Bird [39]):

$$\tau = \tau_y + k\dot{\gamma}^{n-1} \; ; \tau \geq \tau_y$$
$$\dot{\gamma} = 0 \; ; \tau < \tau_y$$

Where k is the consistency index, n is the power-law index and τ_y is the yield stress. The viscosity above the yield stress is given by:

$$\eta = \frac{\tau_y}{\dot{\gamma}} + k\dot{\gamma}^{n-1}$$

2.2.2. Flow Regimes

Wellbore cementing, the common flow regimes through annular spaces are laminar, turbulent, and transitional. Laminar flow occurs when fluid moves in parallel layers, with the central layers flowing faster than those near the casing wall, resulting in minimal interaction between layers. In contrast, turbulent flow involves chaotic velocity fluctuations, breaking down the layers and promoting efficient mixing and displacement, making it the preferred regime for well cementing to effectively displace drilling fluids. Transitional flow represents an intermediate stage, exhibiting both laminar and turbulent characteristics. Additionally, plug flow describes a low-velocity, homogeneous movement, though it is rarely dominant in modern well cementing except in very large boreholes. The identification of these flow regimes relies on Reynolds number analysis, which evaluates fluid behavior based on its flow conditions, determining whether the regime is laminar, turbulent, or transitional (Applied Well Cementing Engineering [40]).

According to Bourgoyne et al. [41] laminar flow occurs for Reynolds numbers below 2100, while Reynolds numbers exceeding 4000 are characteristic of complete turbulent flow through tubes. Flow falling between these values is considered transitional. However, determining flow regimes is frequently more complex than this straightforward classification. Laminar flow has been observed under controlled conditions at Reynolds numbers as low as 1200 and as high as 40,000 (although such extremes are uncommon in typical cementing operations. It is worth mentioning that for non-Newtonian fluids the Reynolds number should be evaluated using a characteristic viscosity, usually determined at a characteristic shear rate of the flow.

2.2.3. Density

Fluid density is a critical property that requires careful analysis during cementing operations. According to Foroushan [18], effective displacements are achieved by maintaining adequate differences in density and viscosity between the displacing and displaced fluids, while ensuring laminar flow during displacement.

Haut and Crook [42] emphasized that there are three distinct types of flow regimes in which non-Newtonian fluids can be classified: laminar, turbulent, and plug flow. The authors concluded that the velocity profile in the laminar regime is not as uniform around the annulus as in plug flow or turbulent regimes. Furthermore, they showed that the effects of density cannot be ignored, as it is precisely the difference in densities between the drilling fluid and the cement slurry that causes instability at their interface.

According to Naccache et al. [43] in eccentric geometries the denser fluid induces fluid transport from larger to narrow side in the azimuthal direction, thereby enhancing the cementing process. This enhancement arises from the flat interface between the two fluids.

McClean et al. [44] also noted that in eccentric annuli, the displacement of cement paste tends to occur predominantly through the wider section of the geometry, while drilling fluid tends to be channeled through the narrower section. This observation is dependent on factors such as fluid densities, pumping rates, and annular geometry. To prevent undesired displacement, the pressure gradient from cement circulation and buoyancy force must exceed that required to remove drilling fluid. Analytical models and experimental data describe this displacement mechanism, showing a "piston-like" displacement under certain conditions.

Ytrehus et al. [5] have shown that significant density variations between the displacing and displaced fluids, particularly in highly inclined wells at low flow rates, improves the buoyancy of the displaced fluid.

Jakobsen et al. [9] developed an experimental setup to replicate a well. This apparatus allowed for adjusting the annulus eccentricity and could be tilted from 0º to 90º. Results from experiments with a 55% eccentricity and a 60º inclination showed that displacement efficiency increases as the density of the displacing fluid becomes higher than the displaced one.

2.2.4. Pipe Eccentricity and Gravity influences

According to Lavrov & Torsæter [45] , inclined and horizontal wells face additional challenges during the displacement process, including gravity-induced eccentricity and particle sedimentation. Eccentricity, which is common in both vertical and inclined wells, can be exacerbated by gravity in inclined wells, further complicating displacement. Figure 7 depicts an instance of particle sedimentation, where gravity affects solid particles (such as barite) in the drilling fluid, causing them to settle and thicken the fluid in the narrow part of the annulus. Displacing thicker drilling fluid may necessitate higher flow rates and increased fluid yield stress, thereby making the displacement process more challenging (Fredheim [2]).
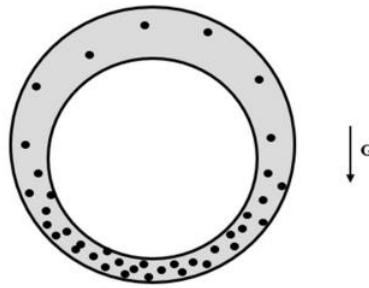
Figure 7 - Solid particles settling and accumulating in inclined or horizontal configurations (Fredheim [2]).

In cementing operations, it is common for the pipe to be off-center in the wellbore (Figure 8). This offset is known as eccentricity and indicates ratio of the distance separating the centers of the cylinders to their radial variance, or the degree which one pipe is positioned away from the center of another pipe. This misalignment can significantly impact on the efficiency and effectiveness of the cementing process. Eccentricity affects fluid dynamics, leading to irregular cement distribution and potentially compromising the structural integrity of the well (Fredheim [2]).
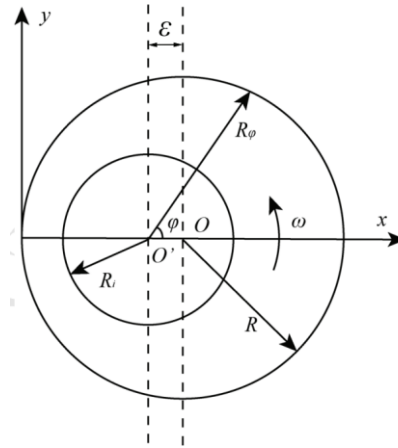
Figure 8 - The schematic diagram of eccentric annulus (Bu et al. [44]).

Eccentricity, or the off-center positioning of casing - especially on the low side of the wellbore - significantly impacts fluid flow dynamics in the annulus. This misalignment can cause uneven fluid displacement during cementing, complicating the achievement of effective zonal isolation necessary for well integrity and preventing fluid migration. While areas with higher flow rates may be properly cemented, other regions could remain inadequately filled, leading to voids or channels that undermine sealing. To ensure successful cement placement and reliable zonal isolation, it is crucial to address eccentricity and consider enhanced cementing techniques or specialized equipment (Moroni et al. [3]).

Figure 9 illustrates these dynamics, highlighting how such conditions can result in varying widths and uneven distribution of fluids within the annular space.
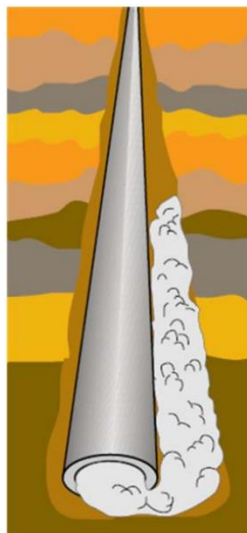
Figure 9 - No flow in the narrow side of the eccentric annulus (Moroni et al. [3]).

For Newtonian fluids, the effects of pipe eccentricity in the profile velocity can be observed in Figure 10.
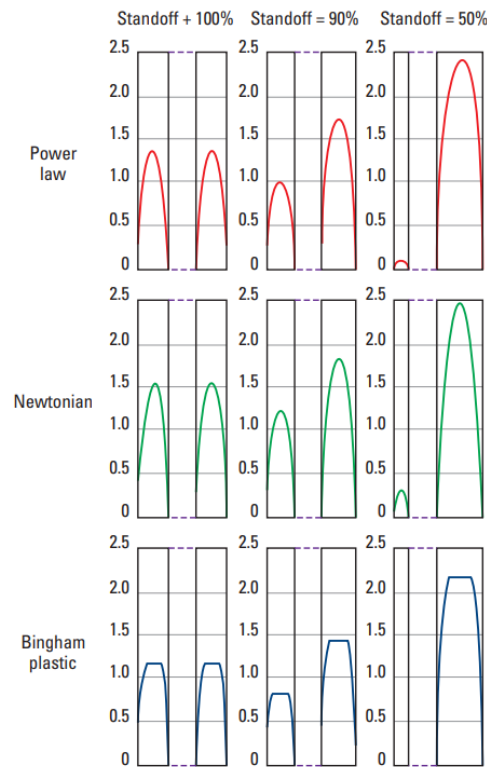
Figure 10 - Typical example of velocity profile on the narrow and wide sides of eccentric annuli for model fluids. Reprinted with permission of SPE (Guillot and Nelson [32]).

Eccentricity significantly affects velocity distribution in annular flow by directing fluid movement toward the wider sections of the annulus, resulting in uneven flow rates that impact displacement efficiency. While increased velocity in the wider areas can enhance turbulence and mixing, improving fluid displacement, the reduced flow velocity in narrower sections can create stagnant zones. This stagnation raises the risk of incomplete cement placement and poor zonal isolation (Guillot and Nelson [32]).

Walton and Bittleston [49] note that the impact of pipe eccentricity on the laminar flow of non-Newtonian fluids is similar to that observed in Newtonian fluids, but predicting these effects is more complex for fluids with yield stress. Figure 11 displays the velocity profiles of a Herschel-Bulkley fluid flowing in annuli with varying eccentricities, along with analytical and numerical solutions for the flow of a Bingham plastic fluid in a narrow eccentric annulus.
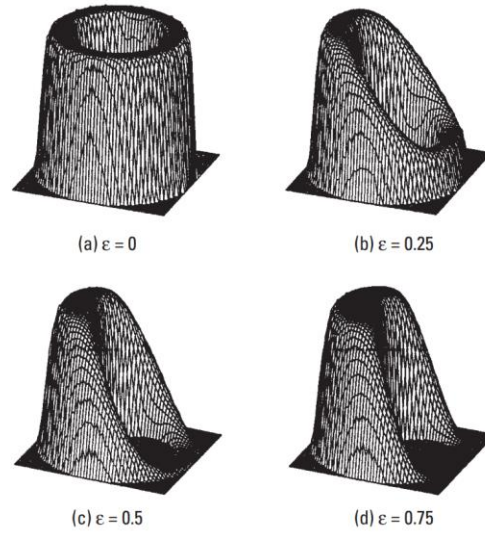
Figure 11 - Velocity profile for a Herschel-Bulkley fluid as a function of eccentricity (Walton and Bittleston [49]).

Figure 11(a) shows the concentric annulus exhibits flat profiles with stress levels below the yield stress; Figure 11 (b) shows a 0.25 offset, indicating a significant velocity reduction on the narrow side compared to the power-law fluid. Figure 11 (c), with a 0.5 offset, demonstrates that flow has completely stopped on the narrow side, while Figure 11 (d) highlights this stagnation and reveals a wider plug forming on the wide side of the annulus (Walton and Bittleston [46]).

The numerical study shows that for a Herschel-Bulkley fluid with yield stress, velocity distortion is especially evident on the narrow side of the annulus, suggesting that the yield stress surpasses the fluid's shear stress. In a horizontal annulus, front displacement is affected by the balance between gravity, which promotes stable stratification, and eccentricity, which directs fluid flow towards the wider section resulting in uneven velocity distribution. Increased velocity in wider areas may improve mixing and displacement efficiency, but reduced velocity in narrower sections can create stagnant zones, hindering effective displacement and leading to incomplete filling (Walton and Bittleston [46]).

3. Methodology

Displacement efficiency through an annular tube is explored in this work. Specifically, the focus is on low Reynolds numbers, where a non-Newtonian fluid (displacing fluid, blue xanthan gum solution) displaces a Newtonian one (displaced fluid, tap water), simulating plug and abandonment operations. The experimental setup consists of a test rig comprising steel tubing enclosed within a transparent casing, replicating realistic dimensions. Two different inclinations (0 and 60° degrees), encompassing both concentric (0%) two eccentric (62% and 75%) configurations are investigated. To assess the impact of various parameters on displacement efficiency, the study employs flow visualization techniques and evaluates interface stability at the experimental apparatus.

3.1. Dimensionless Analysis

The utility of dimensional analysis extends beyond simplification. It enables the scaling of experimental results, allowing findings from model-scale experiments to be applied to full-scale applications by converting complex parameters into dimensionless groups. This approach allows for the reduction of variables, making the analysis more manageable and the results more interpretable.

Bolster, Hershberger, & Donnelly [47] demonstrated the feasibility of establishing connections between analogous systems through the principles of similarity. By converting physical parameters into dimensionless groups, researchers can identify relationships and predict the behavior of different systems under various conditions. This method is essential in engineering and physics, where it enables the scaling of experiments from models to full-scale applications, ensuring that insights gained from small-scale experiments can be reliably applied to larger systems. Dynamic similarity and dimensional analysis, originating from fluid mechanics are used to simplify problems by reducing system parameters. This thesis will utilize both geometrical and dynamic similarity.

3.1.1. Governing Equations

Dimensional analysis is extremely important when attempting to replicate real case into down-scale experiments. The parameters of interest are essentially obtained by making the main variables in the mass conservation and linear momentum equations dimensionless (Naccache et al. [43]).

These parameters are subsequently employed to establish correlations, establishing a link between real-world and laboratory observations. The governing conservation equations of mass and momentum for incompressible purely viscous fluids are comprehensively detailed in equations below forming a theoretical foundation crucial for analyzing and interpreting experimental results.

Mass conservation:

$$\frac{\partial \hat{\rho}}{\partial \hat{t}} + \widehat{\nabla}\left(\hat{\rho} \cdot \widehat{\boldsymbol{v}}\right) = 0 \rightarrow \widehat{\nabla} \cdot \widehat{\boldsymbol{v}} = 0 \tag{1}$$

Momentum conservation:

$$\hat{\rho}\frac{\partial \hat{v}}{\partial \hat{t}} + \hat{\rho}\left(\widehat{\boldsymbol{v}} \cdot \widehat{\nabla}\right)\widehat{\boldsymbol{v}} = -\widehat{\nabla}\hat{p} + \nabla \cdot (\eta\,\widehat{\boldsymbol{v}}) + \hat{\rho}\widehat{\boldsymbol{g}} \tag{2}$$

The non-dimensional equations are given by:

$$\nabla \cdot \boldsymbol{v}^* = 0$$

$$\rho^*\left[\frac{\partial v^*}{\partial t^*} + (\boldsymbol{v}^* \cdot \nabla^*)\boldsymbol{v}^*\right] = -\nabla^* p^* + \frac{1}{Re}\nabla \cdot (\eta^*\,\boldsymbol{v}) \tag{3}$$

The dimensionless governing parameters are shown below:

$Aa_1 = (\pi * D_o{}^2)/4$; Annulus cross-sectional area

$Aa_2 = (\pi * D_i{}^2)/4$; Annulus cross-sectional area

$t_c = \frac{\forall_a}{\dot{\forall}}$; Characteristic time

$\eta^* = \frac{\eta}{\eta_c}$; Characteristic viscosity

$\bar{V} = \frac{\dot{\forall}}{A}$; Caracteristic velocity

$u^* = \frac{u}{\bar{V}}$; Dimensionaless velocity in x direction

$t^* = \frac{t}{t_c}$; Dimensionless time

$p^* = \frac{p}{\rho_2 \bar{V}^2}$; Dimensionless pressure

$x^* = \frac{x}{D_h}$; Dimensionless Longitudinal direction

$\rho_{r=} \frac{\rho_2}{\rho_1}$; Density ratio

$D_h = Do - Di$; Hydraulic Diameter

Di = Inner diameter

Do = Outer diameter

$Re_c = \frac{\rho_2 v_2 D_h}{\eta_c}$; Reynolds numbers of Xanthan Gun

$Re_a = \frac{\rho_a v D_h}{\mu}$; Reynolds numbers of water

$r^* = \frac{r}{D_h}$; Ratio

$\dot{\gamma} = v/D_h$; Shear rate

$\eta_c =$; Viscosity of Xanthan Gum

$\eta_r = \frac{\eta_2}{\eta_1}$; Viscosity ratio

$v^* = \frac{v}{\bar{V}}$; Velocity in y direction

$Fr = U^* \sqrt{At\, g\, D_h}$; Frode number

3.2. Experimental fluids

The experimental investigations were conducted using a fixed pair of model fluids to simulate the displacement process of brine by a cement slurry. The cement slurry, acting as the displacing fluid, was modeled using a non-Newtonian xanthan gum solution (XG), while tap water served as the displaced fluid. All experiments were performed at ambient temperature (~ 20ºC), and the properties measured at the same temperature.

The density of the tap water used in these experiments as a displaced fluid was 998 kg/m³ and a viscosity of 0.001 Pa.s (unites given by literature).

Conversely, the xanthan gum solution (Figure 12) was prepared by mixing xanthan gum at a volumetric proportion of 2% in water containing approximately 223 g/l of salt, resulting in a density of 1130 kg/m³.

Figure 12 - Xanthan Gum solution (2%) being mixed

A mixer was used to blend the fluid. The density of the displaced and displacing fluids was quantified utilizing a Density meter DMA 4100 M, employing the oscillating U-tube method. A sample fluid was introduced into a U-tube glass

apparatus and subjected to vibration at a characteristic frequency to determine the fluid density. The density of the displacing fluid was adjusted by adding salt, while the addition of blue ink assisted in distinguishing between the fluids. Investigations were conducted to evaluate any potential impact of the blue ink on fluid density, with results indicating negligible influence.

The rheological properties of the xanthan gum solution were assessed using a rotational rheometer (Anton Paar Rheoplus/32 V3) equipped with a parallel plate geometry (CP75). In this methodology, the fluid sample was interposed between two plates, with the lower plate undergoing rotational motion at a consistent rate. The upper plate measured the torsional force generated within the fluid sample, facilitating the determination of the stress-strain relationship and subsequently, the viscosity.

A shear rate ramp-down procedure was employed, ranging from 1020 s^{-1} to 0.01 s^{-1}. Rheological measurements were conducted thrice for each sample, ensuring repeatability. The xanthan gum solution exhibited shear thinning behavior and yield stress, thus its rheological characteristics were described using the Herschel Bulkley model, where the viscosity function (η) is defined by:

$$\begin{cases} \dfrac{\tau_y}{\dot{\gamma}} + K.\dot{\gamma}^{n-1} & \text{if } \ \tau \geq \tau_y \\ \infty & \text{if } \tau < \tau_y \end{cases}$$

Where τ_y is the yield stress, K is the consistency index, and n is the power-law index.

Figure 13 presents the flow curve of xanthan gum, highlighting its viscosity behavior at various shear rates, along with the parameters of the corresponding Herschel-Bulkley model. These parameters were obtained by averaging three readings and minimizing the sum of the squares of the shear stress residuals to ensure a precise fit with the experimental data.

The process involved minimizing the sum of the squares of the shear stress residuals, ensuring that the fitted model closely aligns with the experimental data. The fluid shows a yield stress of 6.64 Pa, with K = 2.32 Pa·s^n and n = 0.406.
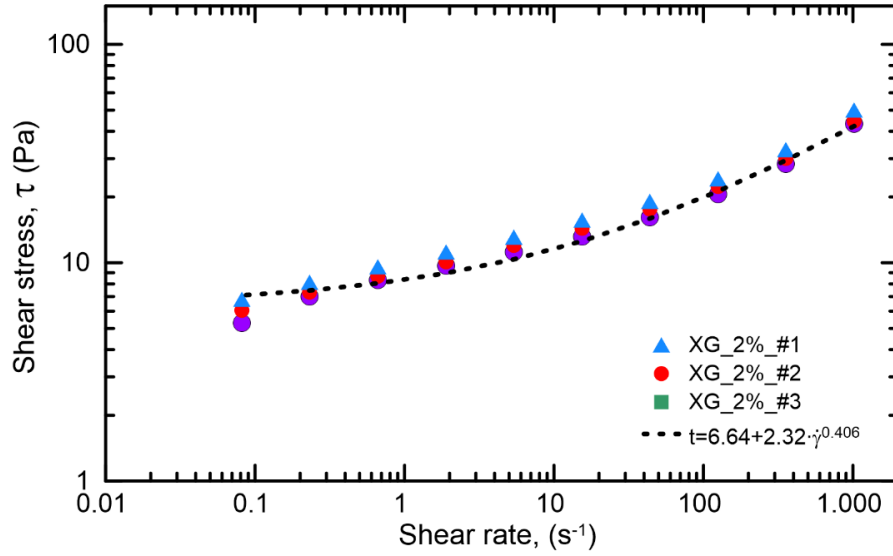
Figure 13 - Flow curve of the XG prior to the displacement tests. The solid line is the corresponding Herschel Bulkley fit to the measurements.

The composition of the fluids was guided by dimensional analysis, whereby fresh water was employed as the primary component for both experimental solutions, owing to its adeptness in dissolving salt weight agents and its attributes as an incompressible Newtonian fluid with reliably low viscosity.

The viscosity ratio and Reynolds numbers are defined in Equations 4,5 and 6:

$$\eta_r = \frac{\eta_c}{\mu} \tag{4}$$

$$Re_c = \frac{\rho_c v D_h}{\eta_c} \tag{5}$$

$$Re_a = \frac{\rho_a v D_h}{\mu} \tag{6}$$

Where η_c represents the viscosity of xanthan gum assessed at a characteristic shear rate of $\dot{\gamma} = v/D_h$, μ denotes the viscosity of tap water, v denotes the average velocity of the fluids at the entrance, D_h denotes the hydraulic diameter of the annular section and ρ_c and ρ_a are density of xanthan gum and water. Reynolds numbers of xanthan gum and water are respectively represented by Re_c and Re_a.

Summary of fluid properties used in the displacement experiments are shown in Table 1:

Table 1 - Summary of fluid properties used in the displacement

Parameter	Symbol	Value
Tap water		Displaced fluid
Density	ρ_1	988 kg/m^3
Viscosity	μ_1	0.001 Pa.s
Xantham Gum		Displacing fluid
Density	ρ_2	1130 kg/m^3
Viscosity	η_c	$(6.64 + 2.32\dot{\gamma}^{0.406})/\dot{\gamma}$ Pa. s
Annulus cross-sectional area:	Aa	0.001845 m
Displacement flow rate (1)	q_1	10 l/min
Shear rate	$\dot{\gamma}_1$	4.63
Velocity	v_1	0.09 m/s
Reynolds Tap water	Rea$_1$	1758
Reynolds Xantham Gum	Rec$_1$	0.84
Frode Number	Fr$_1$	0.83
Atwood Number	At$_1$	0.06
Viscosity Ratio	μ_1 / η_c	0.00042
Displacement flow rate (2)	q_2	20 l/min
Shear rate	$\dot{\gamma}_2$	9.27
Velocity	v_2	0.18 m/s
Reynolds Tap water	Rea$_2$	3517
Reynolds Xantham Gum	Rec$_2$	3.00
Frode Number	Fr$_2$	1.7
Atwood Number	At$_2$	0.06
Viscosity Ratio	μ_1 / η_c	0.00075

3.3. Experimental setup

The experiments were conducted using a test rig located at the Norwegian Research Centre (NORCE) supported by BRANOR project.

The primary objective of these experiments is to accurately replicate the displacement processes observed in real-world cementing operations using a carefully scaled-down laboratory test rig. This rig is equipped with a carefully designed flow loop that displaces two fluids in an annular configuration, effectively simulating real-world field conditions. A positive displacement pump drives the fluids through the annular space, maintaining a consistent flow rate that is precisely controlled by a variable frequency driver.

Additionally, it includes a tool that enables the adjustment of eccentricity, enabling precise mimicry of both concentric and eccentric wellbore situations commonly encountered in actual cementing operations. By recreating these scenarios in a controlled environment, the setup facilitates a detailed analysis of fluid behaviors, interactions, and flow patterns during displacement. This level of precision is critical for understanding how variables like annular geometry and eccentricity influence displacement efficiency and overall, well integrity. Figure 14 illustrates the rig's schematic.

Figure 14 - Schematic of an annular displacement test rig (Fredheim [2])

The overall test setup is shown in Figure 15.
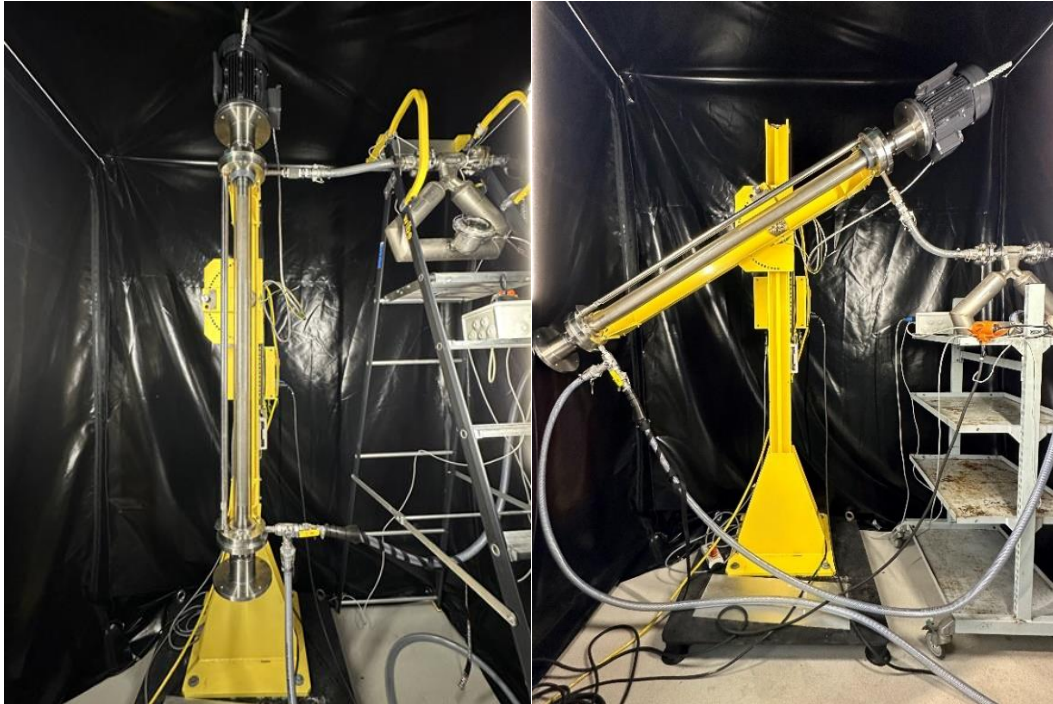
Figure 15 - Picture of the experimental apparatus, captured in both vertical and horizontal orientations.

The outer tube of the rig is constructed from transparent Lexan material, for clear visualization of the displacement process and a steel inner tube. The detailed experimental setup is provided in Table 2:

Table 2 - Experimental setup parameters.

Parameter	Definition	Value
Tubing diameter	(Di)	50.5 mm
Outer pipe diameter	(Do)	70 mm
Hydraulic diameter	(D_h = Do - Di)	19.5 mm
Total test section length	(L)	1516 mm
Vibration frequency	f	5 Hz
Drive shaft offset	e'	1 mm
Annulus Eccentricity, e'	$2\delta/$(OD ID)	0°, 62°, 75°
Inclination	θ	0°, 60°

Figure 16 provides detailed Schematic of lab experimental set up.
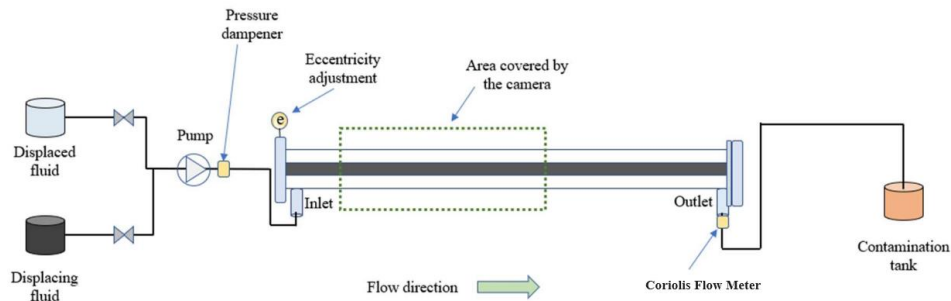
Figure 16 - Schematic of lab experimental set (modified from Fredheim [2]).

A Coriolis flow meter (model CMF100M180N2) was integrated into the test setup to precisely measure flow rate, density, and temperature at the outlet as fluids were displaced through the annulus geometry. This real-time monitoring of critical flow parameters provided valuable insights into the fluid dynamics during displacement. Additionally, flow visualization was performed throughout the experiment using a Nikon D7500 camera to validate the fluid interface during displacement and quantify the fluid remaining near the walls of the annulus. This combination of tools enabled detailed observation and analysis of the displacement process, ensuring a comprehensive understanding of both the fluid interface behavior and the amount of residual fluid.

These measurements were critical for evaluating displacement efficiency and identifying any areas where optimization was needed to improve well integrity and zonal isolation.

The pipe's eccentricity can be adjusted from fully concentric (0% eccentricity) to around 100%. Adjustments are made by manipulating two screws supporting the inner pipe. These screws are controlled using an angle disc with measurements ranging from 0 to 9 mm. The desired eccentricity is maintained along the test section.

The eccentricity is symmetrical around the vertical axis passing through the annulus, ranging from 0° to 180°, representing 0% to 100% eccentricity respectively. Following the adjustment shown in the schematic to set up 70.53

degrees, the screws must be moved to 7 mm corresponding to the 70.53° mark on the disc (Figure 17).
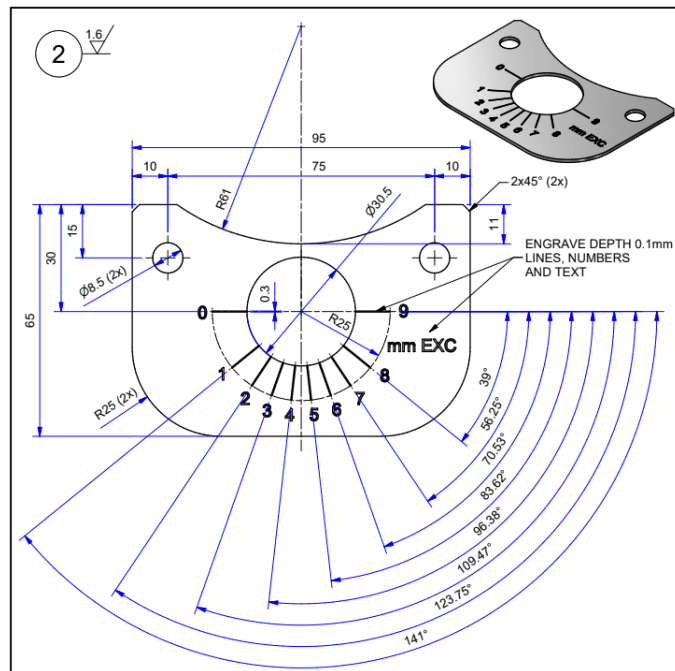
Figure 17 - Eccentricity adjustment

3.3.1. Coriolis Flow meter

The experiments utilized the Coriolis model CMF100M180N2, an advanced flow meter designed to provide precise measurements of mass flow, density, and temperature.

3.3.2. Pump

The test fluids were pumped from the fluid storage tanks to the test rig annulus using a Verderflex Rollit 25 pump. This pump has the capacity of a maximum flow rate of 2200 liters per hour, a maximum pump speed of 165 RPM, and a maximum discharge pressure of 2 bar.

3.3.3. Lab View Software

LabVIEW software integrates with National Instruments hardware for data acquisition and storage, enabling recording of experimental data (Appendix C).

4. Experimental Plan

The experiments aimed to study the impact of vibration on fluid displacement under low flow rates. The density of both fluids was kept constant, while variables such as flow rate, eccentricity, and inclination were adjusted. The dynamic viscosity of the displacing fluid adhered to a rheological model previously discussed, ensuring consistent and predictable flow behavior.

The eccentricity was examined at three levels: concentric (0% eccentricity), and two eccentric configurations at 62% and 75% eccentricity. Inclination was analyzed in two orientations: a vertical position and an inclined position at 60 degrees. Vibration was applied simultaneously during the experiments and maintained at a constant frequency of 5 Hz for all measurements. Two different Reynolds were also investigated (Re 0.84 and Re 3.00).

The experimental plan was structured with the following steps:

1. Preparation of Fluids: Two fluids were utilized in the experiments: a blue-colored Xanthan gum solution representing a cement slurry (displacing fluid) and tap water serving as brine (displaced fluid).

2. Set up of Experimental Apparatus: The experimental setup was configured to accommodate three different levels of eccentricity (0%, 62% and 75%) and two inclinations (0 and 60 degrees inclined).

3. Vibration's frequency: Vibration at 5 Hz frequency was applied consistently across all tests and it was monitored and controlled to maintain uniformity.

4. Variation of Flow Rates: The flow rates were varied systematically to study their interaction with vibration and the other variables. This helped

in understanding how low Reynolds' number conditions affect displacement efficiency.

5. Data Collection and Analysis: Data were collected for each combination of eccentricity, inclination, and flow rate under the influence of vibration. The steps of the experimental plan are shown in more detail in Figure 18.

6. Comparison with Control Tests (Optimal Case): Control tests without vibration were conducted to establish a baseline for comparison. This is useful to isolate the effect of vibration from other factors.

7. Data post-processing and Evaluation of Results: The fluids displacement behavior was assessed based upon evaluation between Coriolis flow meter measures and post displacement images.

Figure 18 provides the steps of the experimental plan:

Figure 18 - Steps of the experimental plan.

5. Results and discussions

This section analyzes flow displacement in terms of dimensionless density ratio (rd) versus dimensionless time, for a single pumped volume, based on experimental data from the Coriolis Flow meter and supplemented with post-displacement images.

The analysis is fundamentally based on the transition curve's delta. Therefore, what truly matters for conducting the result's evaluation is identifying the initial moment when a slight change in density is detected at the top of the system, up until the point when the density ratio stabilizes.

The study defines "optimal displacement" as the condition where the fluid demonstrates piston-like behavior. This means that the displacement fluid approaches the outlet gradually, resulting in a sudden and sharp increase in the density ratio (dr) from 0 to 1 within a short time, ideally near a value of 1. This piston-like response is indicative of a highly controlled displacement process where the interface between the displacing and displaced fluids remains clear and distinct. Such behavior ensures minimal mixing and turbulence of the fluids leading to a good flat interface during the operation.

Achieving this kind of displacement minimizes losses and maximizes the effectiveness of fluid transfer, making it the most desirable outcome in industrial applications.

The density ratio never reaches exactly 1 due to the mixing process, which can result in fluids with slightly different densities. The density of the mixed fluid is influenced not only by the XG ratio but more strongly by the salt fraction.

The pumped volume and the mixing length may be significantly connected, as the dead volume of the tubing from the post-injection annulus to the point where density is measured by the Coriolis meter can affect the measured pumped volume. Thus, the influence of this dead volume explains why the density ratio curve approaches 1 when the pumped volume is near 1 or even exceeds 1 in some cases.

The dimensionless density ratio is defined as:

$$\text{rd} = \frac{\rho - \rho_1}{\rho_2 + \rho_1} \qquad (7)$$

Where:

ρ is the density of the fluids measured by the Coriolis flow meter in dimensionless time

ρ_1 is de the density of tap water

ρ_2 is the density of Xanthan Gum

The volume of the annular space (V) was calculated according to Eq.10:

$$V = \pi \, (R_o^2 - R_i^2) \cdot L \qquad (8)$$

Where R_o is the outer radius of the annular space, R_i is the inner radius of the annular space and L is the length of the rig with representative values established in Table 2.

The Coriolis flow meter was connected to the rig outlet by a hose with 50 cm length and 2.5 cm diameter. The cylinder volume (V_c) was calculated according to Eq. 11:

$$V_c = \pi \cdot r^2 \cdot L \qquad (9)$$

For this study we use two different flows rates: $q_1 = 10$ l/min and $q_2 = 20$ l/min. So, the time to fulfill the rig (one pump volume) is shown in Table 03.

Table 3 - Time to fill the rig

Total time (Loop + Hose)	Time (s)
t_1	18.3
t_2	9.1

The dimensionless time is determined by dividing the experimental (physical) time by the time required to completely fill the annulus once, as given by the following equation: dimensionless time $= t^* = t \: / \: (V_{annulus} \: / \: q)$, where q is the imposed flow rate. I

Initially, the density recorded by the Coriolis flow meter corresponds to that of water, as water is the fluid present in the system at the beginning of the experiment. As the experiment progresses and xanthan gum (XG) begins to flow out of the annulus and into the measuring section of the rig, the density measured by the flow meter starts to increase. This increase in density is attributed to the properties of xanthan gum, which has a higher density than water.

By tracking the density changes throughout the experiment, it enables a better understanding of how effectively the cement slurry (represented by xanthan gum) is replacing the initial fluid (water) within the annular space. This information is crucial for optimizing cementing operations and ensuring successful fluid displacement in real-world applications.

The comparisons were divided as shown in Table 4.

Table 4 - Lab Experiments

Vertical_concentric: Comparison ZY	
Z.1	Re 0.84_VERT_Conc_
Z.2	Re 0.84_VERT_Conc_vib
Y.1	Re 3_VERT_Conc_
Y.2	Re 3_VERT_Conc_vib

60º Inclined_Concentric: Comparison KX	
K.1	Re 0.84_0.6 Inc_Conc_
K.2	Re 0.84_0.6 Inc_Conc_vib
X.1	Re 3_0.6 Inc_Conc_
X.2	Re 3_0.6 Inc_Conc_vib

Vertical_0.62 eccentric: Comparison AB	
A.1	Re 0.84_VERT_0.6_Ecc_
A.2	Re 0.84_VERT_0.6_Ecc_vib
B.1	Re 3_VERT_0.6_Ecc_
B.2	Re 3_VERT_0.6_Ecc_vib

60º Inclined_ 0.62 eccentric: Comparison EF	
E.1	Re 0.84_0.6 Inc_0.6_Ecc_
E.2	Re 0.84_0.6 Inc_0.6_Ecc_vib
F.1	Re 3_0.6 Inc_0.6_Ecc_
F.2	Re 3_0.6 Inc_0.6_Ecc_vib

Vertical_0.75 eccentric: Comparison CD	
C.1	Re 0.84_VERT_0.75_Ecc_
C.2	Re 0.84_VERT_0.75_Ecc_vib
D.1	Re 3_VERT_0.75_Ecc_
D.2	Re 3_VERT_0.75_Ecc_vib

60º Inclined_ 0.75 eccentric: Comparison GH	
G.1	Re 0.84_0.6 Inc_0.75_Ecc_
G.2	Re 0.84_0.6 Inc_0.75_Ecc_vib
H.1	Re 3_0.6 Inc_0.75_Ecc_
H.2	Re 3_0.6 Inc_0.75_Ecc_vib

The experimental plans were divided:

- Comparison ZY:

Z.1 refers to the runs conducted under low Reynolds number (calculated as Re 0.84 according to the parameters settled to this study), in a vertical inclination, with a concentric geometry and no tubing vibration; Z.2 includes tubing vibration.

Y.1 corresponds the runs under high Reynolds number (calculated as Re 3.00 according to the parameters settled to this study), in a vertical inclination, with a concentric geometry and no tubing vibration; Y.2 includes tubing vibration.

- Comparison AB:

A.1 refers to the runs low Reynolds number (calculated as Re 0.84 according to the parameters settled to this study), in a vertical inclination, 62% eccentric and no tubing vibration; A.2 includes with the tubing vibration.

B.1 refers to the runs under high Reynolds number (calculated as Re 3.00 according to the parameters settled to this study), in a vertical inclination, 62% eccentric and no tubing vibration; B.2 includes tubing vibration.

- Comparison CD:

C.1 refers to the runs low Reynolds number (calculated as Re 0.84 according to the parameters settled to this study), in a vertical inclination, 75% eccentric and no tubing vibration; C.2 includes with the tubing vibration.

D.1 refers to the runs under high Reynolds number (calculated as Re 3.00 according to the parameters settled to this study), in a vertical inclination, 75% eccentric and no tubing vibration; D.2 includes tubing vibration.

- Comparison KX:

K.1 refers to the runs under low Reynolds number (calculated as Re 0.84 according to the parameters settled to this study), 60º degrees inclined, with a concentric geometry and no tubing vibration; K.2 includes tubing vibration.

X.1 refers to the runs under high Reynolds number (calculated as Re 3.00 according to the parameters settled to this study), 60º degrees inclined, with a concentric geometry and no tubing vibration; X.2 includes tubing vibration.

- Comparison EF:

E.1 refers to the runs under low Reynolds number (calculated as Re 0.84 according to the parameters settled to this study), 60º degrees inclined, 62% eccentric and no tubing vibration; E.2 includes the tubing vibration.

F.1 refers to the runs under high Reynolds number (calculated as Re 3.00 according to the parameters settled to this study), 60° degrees inclined, 62% eccentric and no tubing vibration; F.2 includes tubing vibration.

- Comparison GH:

G.1 refers to the runs under low Reynolds number (calculated as Re 0.84 according to the parameters settled to this study), 60° degrees inclined, 75% eccentric and no tubing vibration; G.2 includes the tubing vibration.

H.1 refers to the runs under high Reynolds number (calculated as Re 3.00 according to the parameters settled to this study), 60° degrees inclined, 75% eccentric and no tubing vibration; H.2 includes tubing vibration.

5.1. Vertical Case

The analytical data presented in the graphs in this section illustrates the relationship between dimensionless time and the relative density of the fluids at the rig outlet. These values are derived from precise measurements taken by the Coriolis flow meter, which continuously monitors the flow characteristics during the experiment. This analysis is crucial for understanding the efficiency of the fluid displacement process and optimizing cementing operations in practical applications.

5.1.1. Vertical Concentric

In vertical concentric cases (comparison ZY, figure 19), the displacement was efficient, filling the whole annulus gap.

The data from Coriolis flow meter suggest that the runs under low Reynolds number (solid lines blue and red, Figure 19) the density ratio shifts from 0 to 1 in a dimensionless time approximately to one (one pumped volume), could indicate an absence of fluid mixing and a good flat interface during the displacement.

As Reynolds numbers rise to 3.00 (Figure 19, dotted lines red and blue), the density ratio begins to increase before approximately one pumped volume (dimensional time = 1), and this pattern is consistent across all runs. This observation can be explained by the increase in shear stress at higher Reynolds numbers, which leads to a reduction in viscosity. Consequently, it may suggest an interaction between fluid dynamics and vibrations at elevated flow rates.
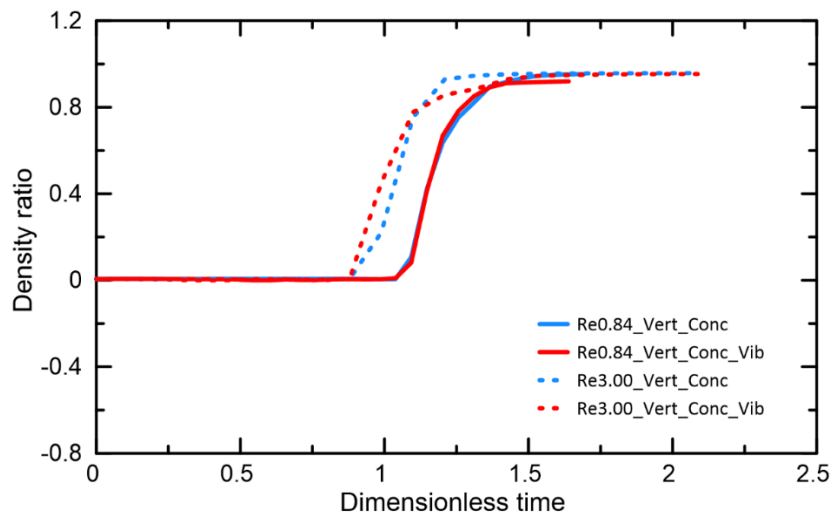
Figure 19 - Comparison ZY

Concentric cases play a crucial role as a baseline for comparison, acting as a critical control to isolate the specific effects of vibration on displacement efficiency. By providing a stable reference point, concentric configurations make it easier to distinguish the direct influence of vibration from other variables, such as variations in flow conditions, pressure changes, or fluid properties. In the absence of vibration, the system's behavior in concentric cases serves as a standard against which the impact of vibration can be measured. This comparison is essential because it ensures that any observed improvements or deviations in displacement efficiency are the result of vibration and not due to unrelated factors or environmental fluctuations.

Moreover, concentric cases help establish a consistent framework for interpreting results across different scenarios, making it possible to accurately quantify the benefits of vibration. Without this baseline, attributing performance changes to specific causes would be speculative and less reliable. By eliminating uncertainties, concentric cases provide a more rigorous and scientifically sound foundation for validating the role of vibration, ultimately enabling a better understanding of how and why vibration influences displacement processes.

Cases Z.1, Z.2, Y.1 and Y.2 show the post displacement images.

Post displacement images – Vertical Cases – Concentric geometry

Case Z.1 - Re0.84_Vert_Conc

Case Z.2 - Re0.84_Vert_Conc_Vib

Case Y.1 – Re3.00_Vert_Conc

Case Y.2 - Re3.00_Vert_Conc_Vib

5.1.2. Vertical Eccentric cases

5.1.2.1. Eccentricity 0.62

In vertical eccentric configurations with an eccentricity of 0.62 (Figure 20, comparisons AB), at Reynolds = 0.84, vibration appears to improve the front displacement process. Specifically, the density transitions from zero to one in approximately one pumped volume with vibration compared to the case without vibration (as shown by solid red and blue lines).

By increasing the Reynolds numbers (dotted lines blue and red), it is possible to observe that the density ratio shifts from 0 to 1 slightly before or equal to one pumped volume dimensionless time (approx.) that might suggest an interplay between the fluids due to increase shear stress leading to viscosity reduction.
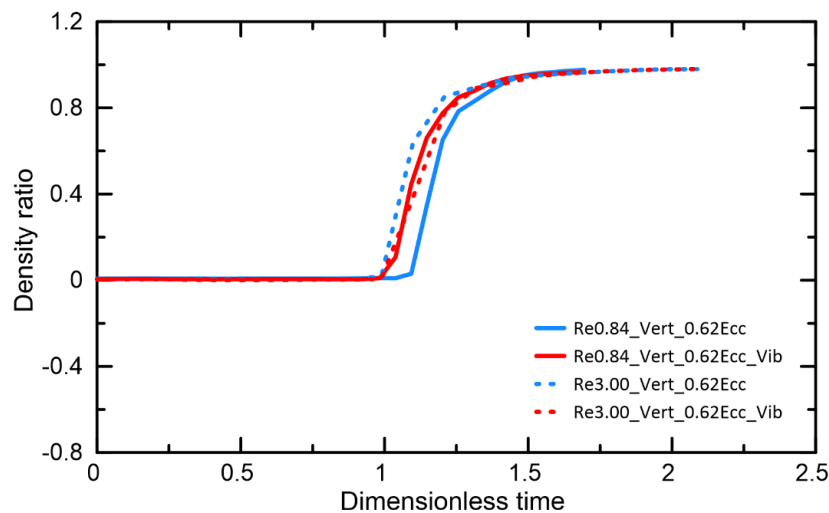
Figure 20 - Comparison AB

Nevertheless, the qualitative analysis of the post-displacement images indicates that the displacement was not fully effective. Despite the presence of vibration, residual water remains trapped in the narrower section of the annulus. This inefficiency is evident in Cases A.1, A.2, B.1 and B.2, where the persistence of water in the confined region suggests incomplete fluid displacement. The inability to fully clear the annulus of water highlights a potential deficit in the displacement process, which could impact overall system performance and efficiency.

Post displacement images – Vertical Cases – 62% eccentric

Case A.1 – Re0.84_Vert_0.62Ecc

Case A.2 - Re0.84_Vert_0.62Ecc_Vib

Case B.1 – Re3.00_Vert_0.62Ecc

Case B.2 - Re3.00_Vert_0.62Ecc_Vib

5.1.2.2. Eccentricity 0.75

With an eccentricity of 0.75 (Figure 21, comparison CD), under the high Reynolds number (Re 3.00), the density ratio starts to increase before dimensionless time of one pumped volume (approx.), which might suggest an interaction between the water and xanthan gum in the loop outlet.

At low Reynolds numbers (Re 0.84, solid lines blue and red), the density transition starts near to one pumped volume and the vibrations appear to offer modest enhancement, as the curve becomes more vertical when compared to the case without vibrations.
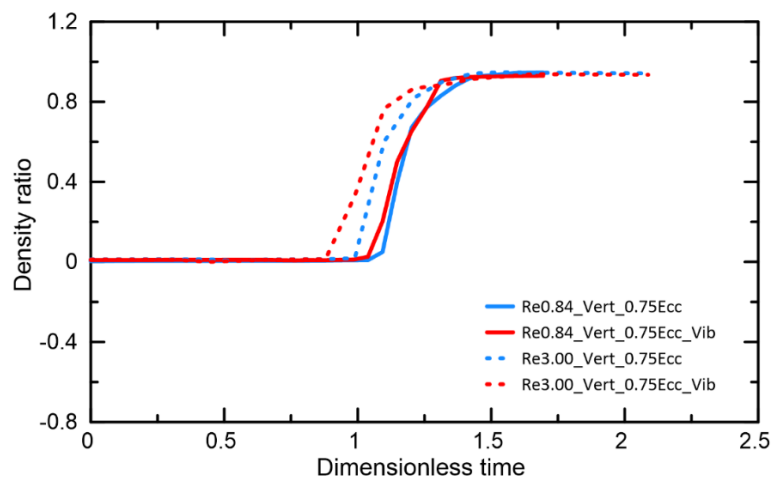
Figure 21 - Comparison CD

However, the post-displacement pictures evidence the presence of water on the narrow side of the annulus, which can be seen in Cases C.1, C.2, D.1 and D.2.

This observation indicates that the applied stress is insufficient to overcome the shear stress necessary to mobilize the trapped water in that region of the annulus. The inadequate stress levels suggest that the force exerted is not strong enough to disrupt the cohesive forces holding the water in place. If the stress remains below the required threshold, the trapped water will continue to hinder fluid flow, leading to reduced efficiency in fluid displacement processes.

Post displacement images – Vertical Cases – 75% eccentric

Case C.1 – Re0.84_Vert_0.75Ecc

Case C.2 - Re0.84_Vert_0.75Ecc_Vib

Case D.1 – Re3.00_Vert_0.75Ecc

Case D.2 - Re3.00_Vert_0.75Ecc_Vib

5.2. Inclined Cases

5.2.1. Concentric

In inclined concentric cases (Figure 22, comparison KX), the density ratio transitions from 0 to 1 within a dimensionless time near to one for all runs and the displacement was efficient, filling the whole annulus gap.
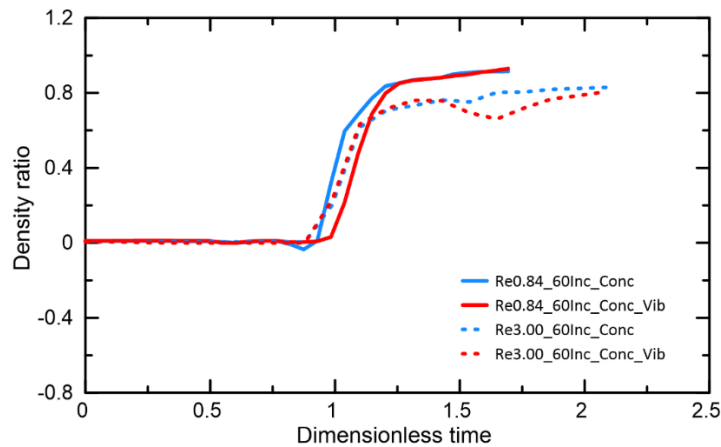
Figure 22 - Comparison KX

Concentric cases provide a crucial baseline for isolating the effects of vibration on displacement efficiency. They serve as stable reference points, allowing researchers to differentiate the influence of vibration from other variables like flow conditions and pressure changes. This comparison ensures that observed improvements in efficiency are attributable to vibration rather than external factors.

Furthermore, concentric cases establish a consistent framework for interpreting results across different scenarios, enabling accurate quantification of vibration benefits. By minimizing uncertainties, they offer a reliable foundation for validating the role of vibration, enhancing understanding of its impact on displacement processes.

Post displacement images are shown in Cases K.1, K.2, X.1 and X.2.

Post displacement images – Inclined Cases - Concentric

Case K.1 – Re0.84_60Inc_Conc

Case K.2 - Re0.84_60Inc_Conc_Vib

Case X.1 – Re3.00_60Inc_Conc

Case X.2 – Re3.00_60Inc_Conc_Vib

5.2.2. Inclined Eccentric cases

5.2.2.1. Eccentricity 0.62

In inclined eccentric cases, 0.62 eccentricity (Figure 23, comparison EF), the same tendency can be observed as the density ratio departs from zero before dimensionless time approximately to one under, high Reynolds Re 3.00 number, that might indicate mixture between the fluids (dotted lines red and blue).

For scenarios under low Reynolds numbers (Re 0.84), the curves behavior is similar regardless of whether vibration is applied, and the density ratio shifts close to one pumped volume.
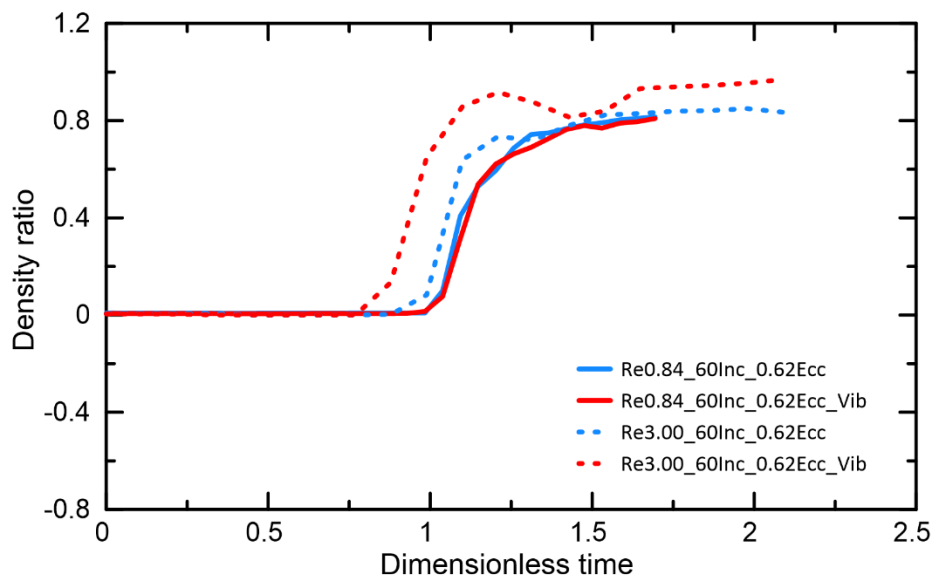
Figure 23 - Comparison EF

Qualitative analysis of the post-displacement images from Cases E.1, E.2, F.1, and F.2 reveals that water continues to accumulate on the narrow side of the annulus. This persistent presence of water strongly suggests that the applied stress is insufficient to exceed the shear stress necessary to mobilize the fluid in that specific region. The inability to generate adequate stress raises concerns about the effectiveness of the displacement process, as it indicates that the forces exerted are not strong enough to overcome the cohesive forces holding the water in place.

Post displacement images Inclined Cases - 62% eccentric
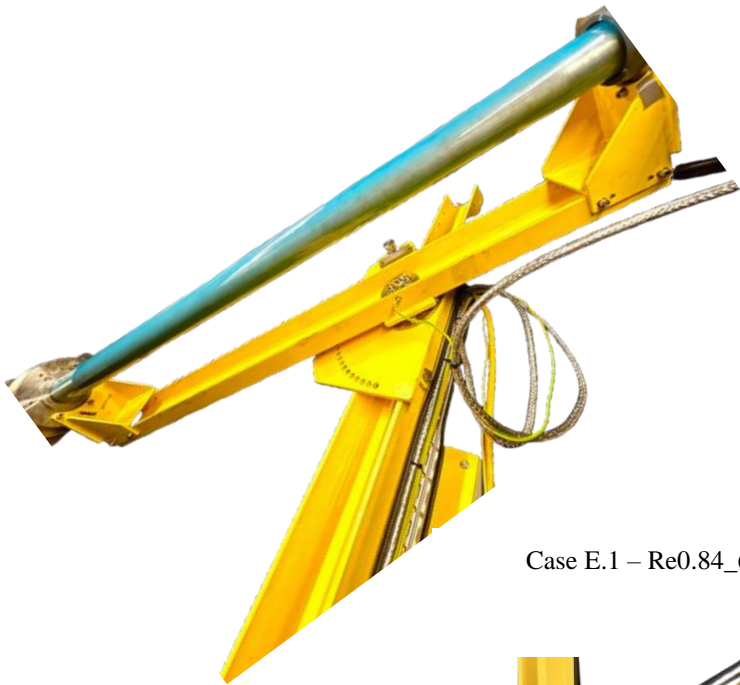
Case E.1 – Re0.84_60Inc_0.62Ecc
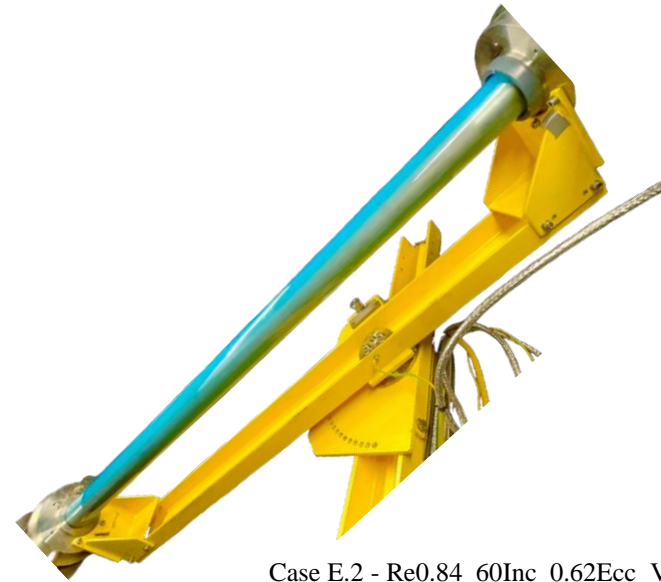
Case E.2 - Re0.84_60Inc_0.62Ecc_Vib

Case F.1 – Re3.00_60Inc_0.62Ecc

Case F.2 – Re3.00_60Inc_0.62Ecc_Vib

5.2.2.2. Eccentricity 0.75

For eccentricity 0.75 (Figure 24, comparison GH), the density ratio begins to increase before dimensionless time of one pumped volume (approx.), which can be understood as a mixture between the fluids under high Re number (Re 3.00, dotted lines red and blue).

At low Reynolds numbers (Re 0.84, solid lines red and blue), vibrations contribute to a slight improvement, as they begin to affect the process slightly earlier than in scenarios without vibration.
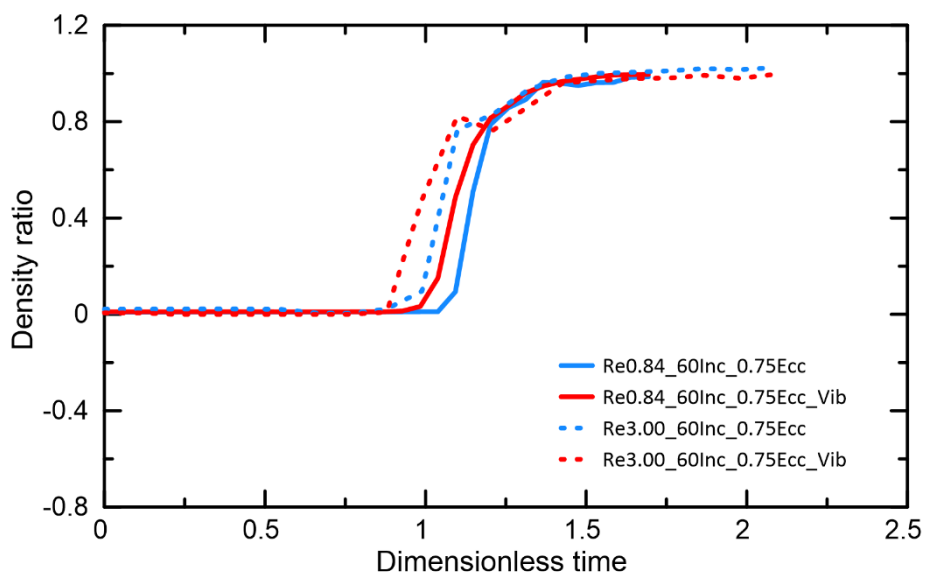
Figure 24 - Comparison GH

However, qualitative data from Cases G.1, G.2, H.1 and H.2 show a water layer remaining in the narrow side of the annulus. This persistent presence suggests that applied stress is inadequate to surpass the shear stress necessary for mobilizing the fluid in that area. The insufficient stress indicates that the forces exerted are not strong enough to overcome the cohesive forces holding the water in place, potentially hindering overall fluid flow and negatively impacting system performance. Therefore, a reevaluation of the applied stress levels may be necessary to improve water mobilization in the annulus.

Post displacement images Inclined Cases - 75%

Case G.1 - Re0.84_60Inc_0.75Ecc

Case G.2 - Re0.84_60Inc_0.75Ecc_Vib
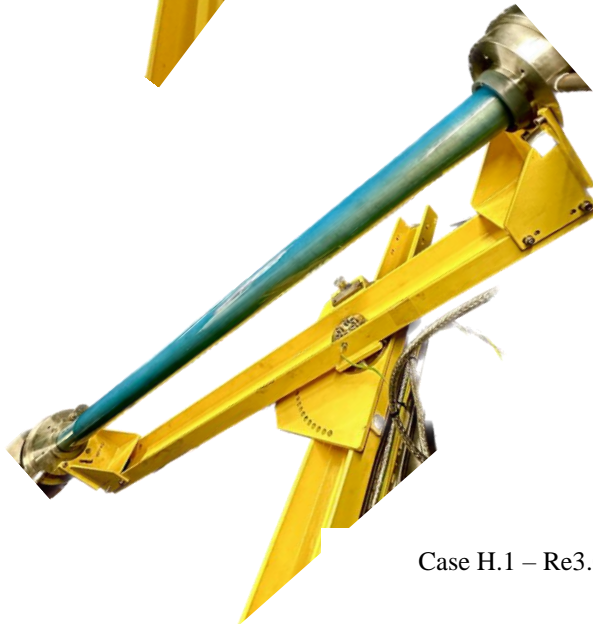
Case H.1 – Re3.00_60Inc_0.75Ecc

Case H.2 - Re0.84_60Inc_0.75Ecc_Vib

6. Conclusion

This study explored the effect of tube vibration on fluid displacement, aiming to determine its potential for disrupting residual layers and improving displacement efficiency. The findings are consistent with previous research, which suggests that vibration can improve front displacement.

In vertical configurations, particularly in eccentric cases with a Reynolds number (Re) of 0.84, data from the Coriolis flow meter indicate that vibration enhances front displacement, indicating a well-defined flat interface between the fluids at the loop outlet. As the Reynolds number increases to 3.00, experimental data reveal a transition in density from zero to one prior to the expected dimensionless time. This could be attributed to the increased shear stress and mixture generated at higher flow rates, leading to greater interaction between the fluids and potentially diminishing the effectiveness of displacement.

In inclined configurations, a comparable pattern emerged. At lower Reynolds numbers, vibration plays a significant role to optimize fluid displacement, likely due to its ability to reduce the influence of residual layers and promote a more uniform flow front. However, as the Reynolds number increased, particularly at Re 3.00, the potential for fluid mixing became more pronounced.

In the eccentric cases, flow visualization reveals that displacement is more effective through the wider region of the annulus, resulting in a higher amount of fluid remaining in the narrow region. However, qualitative post-displacement data shows that a water layer persists along the annulus in eccentric cases, suggesting that the applied vibration in this study may not have been sufficient to mobilize water in the narrow side of the annulus.

Fluid displacement through the narrow side of the system is restricted by insufficient stress levels in that region. The stresses in that region are too low to exceed Xanthan gum's yield stress. As a shear-thinning, viscoelastic material with a defined yield stress, xanthan gum resists flow and deformation when the applied stress is inadequate to surpass this threshold. As a result, the lower stresses in the narrow side prevent the xanthan gum from effectively mobilizing the water.

7. Future work

Future work will involve a comprehensive parametric analysis to gain deeper insights into the effects of various eccentricities, flow rates, and fluid rheologies on displacement efficiency. Specifically, by examining how different degrees of eccentricity influence fluid dynamics, potentially leading to non-uniform cement distribution and compromised well integrity.

Moreover, the rheological properties of various fluids must be investigated to identify formulations that may improve displacement performance in eccentric cases. Understanding how these properties interact with eccentric configurations can lead to the development of more effective cement slurries that ensure consistent and reliable well-bore sealing.

The primary aim of this study is to contribute and even improve academic knowledge by exploring a wider range of parameters and conditions, further enhancing the understanding and optimization of fluid displacement in various industrial applications.

Further research is needed to assess if different vibration frequencies, amplitudes, or patterns could improve results, and to examine how varying fluid properties and flow conditions might influence the effectiveness of displacement.

Additionally, numerical simulations and advanced modeling techniques will be crucial in these investigations, enabling the analysis of a wider range of scenarios and helping to identify the conditions under which vibration can be most beneficial.

We believe that by fostering collaboration and knowledge sharing, these findings can spark further innovation and drive progress in the field, ultimately leading to more efficient and effective fluid displacement strategies.

8. Bibliographic references

[1]   Eslami A, Akbari S, Taghavi SM. An experimental study of displacement flows in stationary and moving annuli for reverse circulation cementing applications. J Pet Sci Eng 2022;213:110321. https://doi.org/10.1016/j.petrol.2022.110321.

[2]   Skadsem HJ, Giljarhus KET, Fredheim FØ, van Riet E, Keultjes WJG. Vibration-assisted annular fluid displacement for rig-less well abandonment operations. J Pet Sci Eng 2022;215:110717. https://doi.org/10.1016/j.petrol.2022.110717.

[3]   Moroni N, Ravi K, Hemphill T, Sairam P. Pipe rotation improves hole cleaning and cement-slurry placement: Mathematical modeling and field validation. Soc Pet Eng - Offshore Eur Oil Gas Conf Exhib 2009, OE 2009 2009;2:1036–46. https://doi.org/10.2118/124726-ms.

[4]   Bu Y, Tian L, Li Z, Zhang R, Wang C, Yang X. Effect of casing rotation on displacement efficiency of cement slurry in highly deviated wells. J Nat Gas Sci Eng 2018;52:317–24. https://doi.org/10.1016/J.JNGSE.2018.01.040.

[5]   Ytrehus JD, Taghipour A. OMAE2017-62028 2018:1–7.

[6]   Vrålstad T, Saasen A, Fjær E, Øia T, Ytrehus JD, Khalifeh M. Plug & abandonment of offshore wells: Ensuring long-term well integrity and cost-efficiency. J Pet Sci Eng 2019;173:478–91. https://doi.org/10.1016/j.petrol.2018.10.049.

[7]   Tao C, Kutchko BG, Rosenbaum E, Massoudi M. A review of rheological modeling of cement slurry in oil well applications. Energies 2020;13. https://doi.org/10.3390/en13030570.

[8]   Lockyear CF, Ryan DF, Gunningham MM. Cement channeling. How to predict and prevent. SPE Drill Eng 1990;5. https://doi.org/10.2118/19865-PA.

[9]   Jakobsen J, Sterri N, Saasen A, Aas B, Kjosnes J, Vigen A. Displacements in eccentric annuli during primary cementing in

deviated wells, 1991. https://doi.org/10.2523/21686-ms.

[10]   Tehrani MA, Bittleston SH, Long PJG. Flow instabilities during annular displacement of one non-Newtonian fluid by another. Exp Fluids Exp Methods Their Appl to Fluid Flow 1993;14. https://doi.org/10.1007/BF00194015.

[11]   Pelipenko S, Frigaard IA. Visco-plastic fluid displacements in near-vertical narrow eccentric annuli: Prediction of travelling-wave solutions and interfacial instability. J Fluid Mech 2004;520. https://doi.org/10.1017/S0022112004001752.

[12]   Malekmohammadi S, Carrasco-Teja M, Storey S, Frigaard IA, Martinez DM. An experimental study of laminar displacement flows in narrow vertical eccentric annuli. J Fluid Mech 2010;649. https://doi.org/10.1017/S0022112009993508.

[13]   Moyers-Gonzalez MA, Frigaard IA. Kinematic instabilities in two-layer eccentric annular flows, part 2: Shear-thinning and yield-stress effects. J Eng Math 2009;65. https://doi.org/10.1007/s10665-008-9260-0.

[14]   Denn MM, Bonn D. Issues in the flow of yield-stress liquids. Rheol Acta 2011;50. https://doi.org/10.1007/s00397-010-0504-3.

[15]   Lindner A, Coussot P, Bonn D. Viscous fingering in a yield stress fluid. Phys Rev Lett 2000;85. https://doi.org/10.1103/PhysRevLett.85.314.

[16]   Aranha PE, Miranda CR, Magalhães JVM, Campos G, Martins AL, Ramalho AB, et al. Dynamic aspects governing cement-plug placement in deepwater wells. SPE Drill. Complet., vol. 26, 2011. https://doi.org/10.2118/140144-PA.

[17]   Tehrani MA, Bittleston SH. Experiments in Huids 5") 1993;256:246–56.

[18]   Foroushan HK, Lund B, Ytrehus JD, Saasen A. Cement placement: An overview of fluid displacement techniques and modelling. Energies 2021;14:1–33. https://doi.org/10.3390/en14030573.

[19]   Aas B, Sørbø J, Stokka S, Saasen A, Godøy R, Lunde Ø, et al. Cement placement with tubing left in hole during plug-and-abandonment operations. JPT, J Pet Technol 2017;69:85–6. https://doi.org/10.2118/0517-0085-jpt.

[20] Skadsem HJ, Kragset S, Sørbø J. Cementing an irregular annulus geometry: Full-scale experiments and 3D simulations. SPE/IADC Drill. Conf. Proc., vol. 2019- March, 2019. https://doi.org/10.2118/194091-ms.

[21] Roustaei A, Frigaard IA. Residual drilling mud during conditioning of uneven boreholes in primary cementing. Part 2: Steady laminar inertial flows. J Nonnewton Fluid Mech 2015;226. https://doi.org/10.1016/j.jnnfm.2015.09.003.

[22] Skadsem HJ, Kragset S, Lund B, Ytrehus JD, Taghipour A. Annular displacement in a highly inclined irregular wellbore: Experimental and three-dimensional numerical simulations. J Pet Sci Eng 2019;172. https://doi.org/10.1016/j.petrol.2018.09.007.

[23] Varges PR, Fonseca BS, De Souza Mendes PR, Naccache MF, De Miranda CR. Flow of yield stress materials through annular abrupt expansion-contractions. Phys Fluids 2020;32. https://doi.org/10.1063/5.0015400.

[24] Varges PR, Rodrigues EC, Moraes LC, de Souza Mendes PR, Naccache MF. Flow instabilities in fluid displacement through enlarged regions in annular ducts. J Nonnewton Fluid Mech 2022;305:104834. https://doi.org/10.1016/J.JNNFM.2022.104834.

[25] Kamali M, Khalifeh M, Saasen A, Godøy R, Delabroy L. Alternative setting materials for primary cementing and zonal isolation – Laboratory evaluation of rheological and mechanical properties. J Pet Sci Eng 2021;201. https://doi.org/10.1016/j.petrol.2021.108455.

[26] Khalifeh M, Hodne H, Saasen A, Vralstad T. Techniques and Materials for North Sea Plug and Abandonment Operations 2013. https://doi.org/10.4043/23915-ms.

[27] Van Riet E, Lucas A, Roijmans R, Keultjes W, Agnew A, Benmesbah MO, et al. Safe, Robust and Efficient Through Tubing Abandonment. SPE - Int Assoc Drill Contract Drill Conf Proc 2023. https://doi.org/10.2118/212530-MS.

[28] Thom F, Angell P, Greig N, Robertson N, Hogg H. Case study for rig-less subsea well abandonment. Soc. Pet. Eng. - SPE/ICoTA Well Interv. Conf. Exhib. 2020, CTWI 2020, 2020. https://doi.org/10.2118/199866-MS.

[29] Thom F, Angell P, Greig N, Robertson N, Hogg H. Case study for rig-less subsea well abandonment. Soc Pet Eng - SPE/ICoTA Well Interv Conf Exhib 2020, CTWI 2020 2020. https://doi.org/10.2118/199866-MS.

[30] Keller SR, Production E. Deviated-Wellbore Cementing : Part 1-Problems 1987:955–60.

[31] Engineering P, Engineering W, Abandonment T-T, Efficiency D, Plug P, Well L, et al. MASTER ' S THESIS n.d.

[32] Nelson EB. Well cementing. Well Cem 1990.

[33] Couturler M, Gulliot D, Hendriks H, Cailet F. Design rules and associated spacer properties for optimal mud removal in eccentric annuli. Annu Tech Meet ATM 1990 1990:1121–8. https://doi.org/10.2118/21594-ms.

[34] Bugrayev A, Singh RK, Nafikova S, Akhmetzianov I, Gurbanov G, Rovshenov G, et al. Mud-removal efficiency boost by engineered scrubbing spacer in cementing operations at Caspian Sea. Soc. Pet. Eng. - SPE Annu. Casp. Tech. Conf. 2021, CTC 2021, 2021. https://doi.org/10.2118/207013-MS.

[35] Aghajannezhad P, Sellier M, Becker S. Patching Hele-Shaw Cells to Investigate the Flow at Low Reynolds Number in Fracture Networks. Transp Porous Media 2021;136. https://doi.org/10.1007/s11242-020-01505-x.

[36] Eslami A, Akbari S, Taghavi SM. An experimental study of displacement flows in stationary and moving annuli for reverse circulation cementing applications. J Pet Sci Eng 2022;213:110321. https://doi.org/10.1016/J.PETROL.2022.110321.

[37] Flumerfelt RW. LAMINAR DISPLACEMENT OF NON-NEWTONIAN FLUIDS IN PARALLEL PLATE AND NARROW GAP ANNULAR GEOMETRIES. Soc Pet Eng AIME J 1975;15. https://doi.org/10.2118/4486-pa.

[38] Nguyen TT. Displacement of Non-Newtonian Fluids in Annular Spaces Tri Thanh Nguyen 2018.

[39] Schechter RS. Transport Phenomena (Bird, R. Byron; Stewart, Warren E.; Lightfoot, Edwin N.). J Chem Educ 1961;38.

https://doi.org/10.1021/ed038pa640.

[40] Liu G. Applied Well Cementing Engineering. 2021. https://doi.org/10.1016/B978-0-12-821956-0.09991-0.

[41] Bourgoyne AT, Millheim KK, Chenevert ME, Young FS. Applied Drilling Engineering. 1986. https://doi.org/10.2118/9781555630010.

[42] Haut RC, Crook RJ. LABORATORY INVESTIGATION OF LIGHTWEIGHT, LOW-VISCOSITY CEMENTING SPACER FLUIDS. JPT, J. Pet. Technol., vol. 34, 1982, p. 1828–34. https://doi.org/10.2118/10305-PA.

[43] Naccache MF, Mieles Pinto HA, Abdu A. Flow displacement in eroded regions inside annular ducts. J Brazilian Soc Mech Sci Eng 2018;40. https://doi.org/10.1007/s40430-018-1342-y.

[44] McLean RH, Manry CW, Whitaker WW. Displacement Mechanics in Primary Cementing. J Pet Technol 1967;19:251–60. https://doi.org/10.2118/1488-pa.

[45] Lavrov A, Torsæter M. Knowledge Gaps and Outstanding Issues. SpringerBriefs Pet. Geosci. Eng., 2016. https://doi.org/10.1007/978-3-319-43165-9_7.

[46] Walton IC, Bittleston SH. The axial flow of a bingham plastic in a narrow eccentric annulus. J Fluid Mech 1991;222. https://doi.org/10.1017/S002211209100099X.

[47] Bolster D, Hershberger RE, Donnelly RJ. Dynamic similarity, the dimensionless science. Phys Today 2011;64. https://doi.org/10.1063/pt.3.1258.

Appendix A

Table 5 - Calculation of experiment variables

<table>
<tr><td colspan="9" align="center">NORCE'S LAB SCALE</td></tr>
</table>

GEOMETRY		
	mm	**m**
Tubbing diameter, Dt	50.5	0.0505
Casing	70	0.07
Dh	19.5	0.0195

Annulus cross-sectional area:		
A1= (πD2^2)/4	0.003847	m
A2= (πD1^2)/4	0.002002	m
Aa	**0.001845**	m

Fluid	**l/min**	**m3/s**
Flow rate - Q1	10	0.00017
Flow rate - Q2	20	0.00033
v1 = Q1/Aa	**0.09**	**m/s**
v2 = Q2/Aa	**0.18**	**m/s**

Excentricity	0.6	

π	3.14	

Pipe rig Lenght (L)	1.516	m

ρ Water	998	kg/m3
ρ XG (2%)	1.130	kg/m3

μ1 (Water ~10ºC)	0.0010	Pa.s
μ2 (XG 2%)	2.37	Pa.s

Experiment							
gpt(γ')	v1	eta (η)	Re1 (water)	Re2 (XG)	μ1/μ2	At	Fr
4.633645697	0.09	2.37	1758.42	0.84	0.00042	0.06	0.83

ρ Water	998	kg/m3
ρ XG (3%)	1.130	kg/m3

μ1 (Water ~10ºC)	0.001	Pa.s
μ2 (XG)	1.33	Pa.s

Experiment							
gpt(γ')	v2	eta (η)	Re1 (water)	Re2 (XG)	μ1/μ2	At	Fr
9.267291394	0.18	1.33	3516.84	3.0	0.00075	0.06	1.7

Appendix B

Table 6 - Calculation of field case variables

<table>
<tr><td colspan="3" align="center">FIELD CASE SCALE</td></tr>
</table>

GEOMETRY	mm	m
Tubbing diameter, Dt	139.7	0.1397
Casing	168.3	0.1683
Dh	28.6	0.0286

Annulus cross-sectional area:		
A1= (πD2^2)/4	0.022235039	m
A2= (πD1^2)/4	0.0153201	m
Aa	0.006915	m

Fluid	l/min	m3/s
Flow rate (2) - Q1	300	0.005
Flow rate (3)- Q2	1000	0.016666667
v1 = Q1/Aa	0.72	m/s
v2 = Q2/Aa	2.41	m/s

Excentricity	0.6	
π	3.14	

ρ Brine	1.030	kg/m3
ρ Slurry	1.920	kg/m3

μ1 (Brine)	0.0010	Pa.s
μ2 (Slurry)	1.7	Pa.s

Field Case							
gpt(γ')	v1	eta (η)	Re1 (Brine)	Re2 (Slurry)	μ1/μ2	At	Fr
25.28235731	0.72	1.73	21300.36	23	0.00058	0.301695	2.485

ρ Brine	1.030	kg/m3
ρ Slurry	1.920	kg/m3

μ1 (Brine)	0.0010	Pa.s
μ2 (Slurry)	1.72	Pa.s

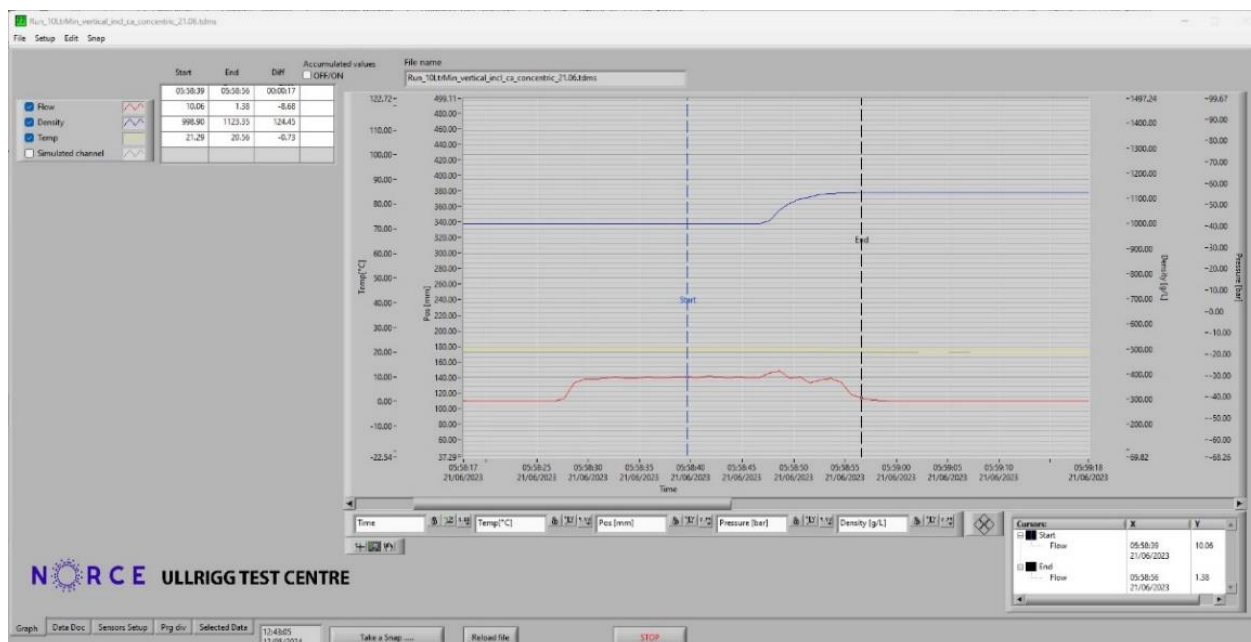| Field Case							
gpt(γ')	v2	eta (η)	Re1 (Brine)	Re2 (Slurry)	μ1/μ2	At	Fr
84.27452437	2.41	1.72	71001.19	77	0.00058	0.30	8.28

Appendix C

Figure 25 - Print Screen of LabVIEW Software